

Old Dominion University

ODU Digital Commons

Electrical & Computer Engineering Theses & Dissertations

Electrical & Computer Engineering

Summer 2013

Improving the Efficiency of P3HT:ICBA Organic Solar Cells by Modifying the Photoactive Solution Preparation Step

Matthew Blaine Samson
Old Dominion University

Follow this and additional works at: https://digitalcommons.odu.edu/ece_etds



Part of the [Polymer and Organic Materials Commons](#), [Polymer Science Commons](#), and the [Power and Energy Commons](#)

Recommended Citation

Samson, Matthew B.. "Improving the Efficiency of P3HT:ICBA Organic Solar Cells by Modifying the Photoactive Solution Preparation Step" (2013). Master of Science (MS), Thesis, Electrical & Computer Engineering, Old Dominion University, DOI: 10.25777/b2r9-3m06
https://digitalcommons.odu.edu/ece_etds/510

This Thesis is brought to you for free and open access by the Electrical & Computer Engineering at ODU Digital Commons. It has been accepted for inclusion in Electrical & Computer Engineering Theses & Dissertations by an authorized administrator of ODU Digital Commons. For more information, please contact digitalcommons@odu.edu.

**IMPROVING THE EFFICIENCY OF P3HT:ICBA ORGANIC
SOLAR CELLS BY MODIFYING THE PHOTOACTIVE SOLUTION
PREPARATION STEP**

by

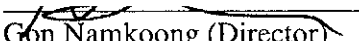
Matthew Blaine Samson
B.S. May 2012, Old Dominion University

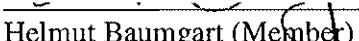
A Thesis Submitted to the Faculty of
Old Dominion University in Partial Fulfillment of the
Requirements for the Degree of

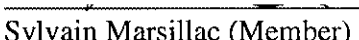
MASTER OF SCIENCE
ELECTRICAL AND COMPUTER ENGINEERING

OLD DOMINION UNIVERSITY
August 2013

Approved by:


Gon Namkoong (Director)


Helmut Baumgart (Member)


Sylvain Marsillac (Member)

ABSTRACT

IMPROVING THE EFFICIENCY OF P3HT:ICBA ORGANIC SOLAR CELLS BY MODIFYING THE PHOTOACTIVE SOLUTION PREPARATION STEP

Matthew Blaine Samson
Old Dominion University, 2013
Director: Dr. Gon Namkoong

Organic solar cells (OSCs) are a promising alternative to conventional silicon solar cells. These organic devices offer the promise of facile low cost large scale solution based processing on lightweight, flexible, plastic substrates. At the present state of the technology, however, OSCs exhibit relatively low power conversion efficiencies. To improve these efficiencies, new materials are constantly being developed.

One such material is the fullerene indene- C_{60} bisadduct (ICBA). When implemented in a poly(3-hexylthiophene-2, 5-diyl) (P3HT) : ICBA bulk heterojunction solar cell, these devices exhibit open circuit voltages exceeding 0.8 V, a value much higher than the devices made implementing phenyl- C_{61} -butyric acid methyl ester (PCBM) which exhibit open circuit voltages of about 0.6 V. This increase in open circuit voltage (V_{OC}) leads to an increase in device efficiency. However, ICBA experiences solubility problems in common organic solvents; thus, special care must be taken in the preparation of P3HT:ICBA photoactive solution. This thesis explores several preparation techniques including sonication, adding solvent additives, stirring and sonicating separately, and mixed solvents.

Solar cells were fabricated using seven P3HT:ICBA solutions prepared differently. Current density-voltage (JV) measurements were done to characterize photovoltaic performance. Fitting was done to extract diode parameters for more in depth

electrical characterization. Atomic force microscopy (AFM), HIROX imaging, and X-ray diffraction (XRD) measurements were done to determine physical properties of the cast thin films. Ultraviolet-visible (UV-Vis) absorption spectroscopy was done to observe optical properties of the solar cells. It was found that sonicating the P3HT:ICBA solution prior to stirring produced the most efficient device due to superior electrical, physical, and optical properties while further improvements were found after using the solvent additive octanedithiol (ODT).

Copyright, 2013, by Matthew Blaine Samson, All Rights Reserved.

ACKNOWLEDGMENTS

I thank my teacher, mentor, and advisor, Dr. Gon Namkoong, for working with me over the past two years. Thank you for allowing me to work in your lab and guiding my research. I also thank my committee members, Dr. Helmut Baumgart and Dr. Sylvain Marsillac, for providing input during the writing and completion of this thesis. I would also like to thank Dr. Tarek Abdel-Fattah for allowing me to use his lab's equipment in the early data collecting stage of this work.

I would like to thank all of my coworkers in the lab. Special thanks to Kevin Latimer, Kurnia Foe, and Pat Boland for teaching me the fabrication process and all required lab maintenance tasks. I am truly indebted to Pat for providing much support in the lab. He has provided so much help in the maintenance of the lab facility; namely in the repair of our e-beam evaporator, our glove box, and our RIE system. Thank you, Pat, for always making time to work with me as I tried to maintain the lab. Dr. Wei Cao was also very helpful in the collection of AFM and XRD data. I graciously acknowledge the William & Mary Applied Research Center Surface Characterization Lab, especially Nick Moore for assisting in the collection of HIROX images. I would also like to thank Jessica Walker and Pam Foshee for administrative support in the purchase of required materials.

I also thank my parents, Marlon and Romina, for always supporting me in my education and other personal endeavors. I thank my sister Malerie and the rest of my family and friends for uplifting my spirit. Finally, I would like to thank God for truly blessing me with a good education and giving me all of the wonderful opportunities I have had.

TABLE OF CONTENTS

	Page
LIST OF TABLES	vii
LIST OF FIGURES	viii
Chapter	
1. INTRODUCTION	1
1.1 MOTIVATION	1
1.2 ORGANIC SOLAR CELL HISTORY	3
1.3 THESIS OBJECTIVES	5
1.4 THESIS OVERVIEW	6
2. ORGANIC SOLAR CELL THEORY	7
2.1 POLYMER MATERIAL	7
2.2 FULLERENE MATERIAL	7
2.3 DEVICE ARCHITECTURE	12
2.4 OPERATION	14
3. FABRICATION PROCESS AND CHARACTERIZATION METHODS	16
3.1 ORGANIC SOLAR CELL FABRICATION PROCESS	16
3.2 ELECTRICAL CHARACTERIZATION	19
3.3 PHYSICAL CHARACTERIZATION	20
3.4 OPTICAL CHARACTERIZATION	21
4. RESULTS, ANALYSIS, AND DISCUSSION	22
4.1 ELECTRICAL PROPERTIES	22
4.2 PHYSICAL PROPERTIES	29
4.3 OPTICAL PROPERTIES	35
4.4 SUMMARY OF DEVICE PERFORMANCE	39
5. CONCLUSION AND FUTURE WORK	46
5.1 CONCLUSION	46
5.2 FUTURE WORK	47
REFERENCES	49
APPENDIX: COPYRIGHT PERMISSIONS / AUTHORIZATIONS	51
VITA	53

LIST OF TABLES

Table	Page
1.1. Costs of materials used in organic solar cell manufacturing	5
2.1. Several fullerene materials including LUMO level and exhibited V_{OC}	10
3.1. P3HT:ICBA solution preparation parameters.....	17
4.1. Photovoltaic properties of the devices shown in Figure 4.1	23
4.2. Photovoltaic properties with different sonication treatments	24
4.3. Photovoltaic properties for mixed solvent active solutions	26
4.4. Extracted solar cell parameters for the mixed solvent experiment.....	26
4.5. Photovoltaic properties for the solvent additive experiment	28
4.6. XRD peak information of the sonication experiment.....	33
4.7. XRD peak information of the mixed solvent experiment.....	35
4.8. UV-Vis peak position, intensity, and total area under curve for different sonication treatments.....	36
4.9. UV-Vis peak position, intensity, and total area under curve for mixed solvents	38

LIST OF FIGURES

Figure	Page
1.1. Timeline of research lab OSC efficiencies between 2001 and 2012	4
2.1. The monomer unit of P3HT	7
2.2. The molecular structure of PC ₆₀ BM	8
2.3. Molecular structure of ICBA indenefullerene	11
2.4. The evolution of OSC architectures.....	13
2.5. Energy band diagram of the P3HT:IC ₆₀ BA solar cell of interest on the left. Energy values are given in eV and are from [4, 11]. Experimental device architecture not to scale on the right.....	14
2.6. Operation of an OSC.....	15
4.1. An initial comparison of the JV plots of IC ₆₀ BA and PC ₆₀ BM Photovoltaic devices	22
4.2. JV curves comparing sonication treatments of P3HT:ICBA devices	24
4.3. JV curves for the mixed solvent experiment.....	26
4.4. JV curves for the solvent additive experiment.....	28
4.5. 1 μm x 1 μm AFM scans of the studied thin films for the sonication treatment experiment on the left. RMS roughness for the thin films is shown in the bottom right of the scans. HIROX images on the right.....	30
4.6. 1 μm x 1 μm AFM scans of the studied thin films for the mixed solvent experiment on the left. RMS roughness for the thin films is shown in the bottom right of the scans. HIROX images on the right	31
4.7. XRD spectra of the sonication experiment	32
4.8. XRD spectra of the mixed solvent experiment.....	34

4.9.	UV-Vis absorption spectra for different sonication treatments	36
4.10.	UV-Vis absorption spectra for mixed solvents	38
4.11.	Summary of the electrical properties of the sonication treatment experiment	39
4.12.	Summary of the physical properties of the sonication treatment experiment including the effect of (a) RMS roughness (b) XRD peak intensity and (c) XRD peak area.....	40
4.13.	Summary of the optical properties of the sonication treatment experiment including the effect of (a) absorbance peak intensity and (b) total absorbance area.....	41
4.14.	Summary of (a) the electrical properties and (b) the extracted diode parameters of the mixed solvent experiment	43
4.15.	Summary of the physical properties of the mixed solvent experiment including the effect of (a) RMS roughness (b) XRD peak intensity and (c) XRD peak area.....	44
4.16.	Summary of the optical properties of the mixed solvent experiment including the effect of (a) absorbance peak intensity and (b) total absorbance area.....	45

CHAPTER 1

INTRODUCTION

1.1 Motivation

With constantly increasing gas prices, fears of depleting future generations' natural resources, and demands for cleaner energy, the need for reliable alternative energy sources is at an all time high. Renewable energy sources including solar, wind, hydropower, geothermal, and biomass are increasingly becoming viable alternatives. These energy sources are considered renewable as they are replenished naturally with virtually infinite supply. Wind energy, hydropower, and geothermal energy can be reliable and cost-effective; however, these forms of energy are dependent on resources which may not be available everywhere. Wind farms should be located in windy areas to ensure steady production of electricity. Hydroelectric dams can only be built where flow of water is sufficient to turn turbines. Geothermal power plants can only be built where geothermal reservoirs are located. Additionally, these alternative energy sources can be difficult to scale from small localized applications to large utility plants.

Solar energy can be readily used everywhere with multiple applications. Home solar water heaters can be used even in cold locations by using antifreeze solutions to heat water. Passive solar building design can be implemented in any building to provide effective building lighting, heating, and cooling. Photovoltaic cells are easily used to power small scale remote locations or large scale grid utility plants. Even on cloudy days or at night, photovoltaic cells can be used to store electricity in battery banks to be used on demand. Thus, photovoltaic cells are an attractive renewable energy source.

Conventional solar cells are typically made of some inorganic semiconductor such as silicon. Fabrication processes to make these inorganic solar cells are usually complex, requiring many steps thereby increasing costs. Additionally, silicon substrates are rigid and inflexible limiting applications [1]. Organic solar cells, a recently developed technology, aim to overcome these limitations of inorganic solar cells. These OSCs are potentially cheaper to fabricate in large volumes due to simpler solution-based processing. Moreover, these OSCs can be fabricated on flexible plastic substrates leading to many novel applications [2, 3].

However, OSC technology does have some drawbacks. Perhaps most importantly, organic semiconductors exhibit charge-carrier mobilities several orders of magnitude lower than those of inorganic semiconductors [3, 4, 5]. However, these low mobilities are slightly balanced by high absorption. Additionally, excitonic diffusion length, to be discussed in more detail in the following chapter, is extremely small requiring thin device architectures -- another problem slightly balanced by high optical absorption. Photoactive polymers also have higher optical band gaps limiting the amount of usable solar spectrum [4]. Organic materials are also instable in ambient conditions; thus, means of sealing OSCs to protect the device from premature degradation are important [2]. Thus, any means to increase device efficiency is considered a viable approach in the field of OSC research. In this thesis, a new material will be discussed which can be used to increase OSC device efficiency.

1.2 Organic Solar Cell History

Organic materials exhibiting a photovoltaic effect were first observed in the 1950s when Kallmann and Pope sandwiched anthracene between electrodes and subjected it to light [5, 6]. Research quickly turned to molecular pigments and dyes such as chlorophyll, phthalocyanine, perylene, and porphyrin which could be incorporated into photovoltaics [4, 6]. In the 1970s, conductive conjugated polymers were discovered. Further breakthrough in OSC technology came in 1985 when fullerene materials were discovered [6]. Tang introduced the concept of a bulk heterojunction (BHJ) and applied it to a dye solar cell in 1986. This BHJ device exhibited a PCE of 1%, a value much higher than the devices at the time [5, 6]. By combining these concepts of conjugated polymers, fullerenes, and the bulk heterojunction, Sariciftci created the first polymer:fullerene OSC [6]. Thus, this technology is a relatively young technology which makes up less than 0.8% of the photovoltaic market compared to the well-studied domain of silicon technologies which made up 92.3% of the market as of 2010 [7].

Currently, the highest efficiency obtained using OSC technology is about 11% as seen in Figure 1.1 which is much lower than conventional semiconductor technologies which exhibit efficiencies greater than 20% [8]. This lower PCE is typically attributed to poor charge transport and high carrier recombination due to the highly disordered nature of the solar cell architecture [3, 4, 5]. However, as Figure 1.1 shows, research on this technology was only really started in the early 2000s whereas other technologies were researched in the 1970s during the semiconductor boom [1, 8]. Thus, there is much hope in the research community that OSC technology will one day achieve efficiencies comparable to inorganic technologies.

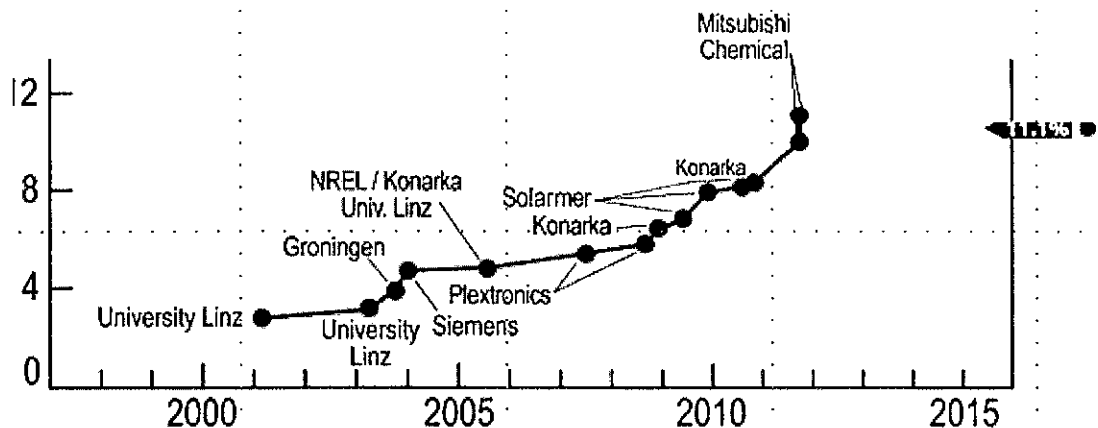


Figure 1.1: Timeline of research lab OSC efficiencies between 2001 and 2012 [8].

Despite the lower efficiencies discussed above, interest in OSC technology remains due to several attractive features. As stated previously, OSC devices can be cheaply fabricated on lightweight, flexible, plastic substrates [2]. Additionally, because it is solution processable, OSC technology can be easily upscaled for large-scale volume processing or even roll-to-roll printing [3]. Thus, it is the aim of researchers in the field to continue to increase PCE while developing processing technologies easily adopted for commercialization.

As stated before, OSC technology has the potential to become a much cheaper alternative to silicon technology. As such, a brief economic description will be given. In 2009, it was estimated that the manufacturing cost of organic solar cells would be between \$50 and \$140 per square meter. Assuming 5% PCE and a 5 year lifetime, this leads to a levelized cost of electricity between \$0.49 and \$0.85 per kWh. These prices are not competitive, and it is estimated that efficiencies of 15% and lifetimes of 20 years are needed to compete. Table 1.1 below lists the material costs which lead to the above figures. While the necessary organic semiconductors may be expensive, such a little

amount is used in the actual solution processing that the costs per square meter are relatively low. As seen in Table 1.1, a major contributor to manufacturing costs is the ITO substrate. As such, other alternative substrates are being researched [9].

Table 1.1: Costs of materials used in organic solar cell manufacturing [9]

Material Function	Material	Maximum Costs (\$/m ²)
Semiconductor	P3HT, PCBM	5
Electrical Contacts	Aluminum, Silver Paint	5
Substrate	ITO	13.68
Protective Covering	Flexible encapsulants	4.40
Sealant	Surlyn	4.40
Total		32.48

1.3 Thesis Objectives

The main goal of this thesis is to compare several photoactive solution preparation methods, such as ultrasonication and using mixed solvents, for P3HT:ICBA solar cell fabrication in terms of their effects on photovoltaic performance in order to determine which of the suggested preparation techniques produces the solar cell with the highest efficiency. To do so, polymer and fullerene basics, organic solar cell device architecture, and device operation are first explained. Additionally, the method used to fabricate organic solar cell devices is detailed. Finally, fabricated solar cells are compared in terms of the effects of electrical, physical, and optical properties on photovoltaic device performance.

1.4 Thesis Overview

This thesis is organized as follows. Chapter 2 discusses the underlying theory of organic solar cells. It details the polymer and fullerene materials of interest, typical device architectures, and operating principles of organic solar cells.

Chapter 3 presents the experimental procedures used in gathering data for this thesis. It details the fabrication process and describes the characterization methods used.

Chapter 4 contains the experimental results, analysis, and discussion. It presents observed electrical, physical, and optical properties of the fabricated organic solar cells. It also attempts to link underlying electrical, physical, and optical properties to the overall photovoltaic properties of the solar cells.

Chapter 5 concludes this thesis by summarizing the work. It proposes possible future work to be done in this specific field.

CHAPTER 2

ORGANIC SOLAR CELL THEORY

2.1 Polymer Material

First, the basic concepts of polymers and fullerenes will be described. A polymer is a hydrocarbon material with a structure based off of a repeating monomer unit. However, not all polymers may be used for OSC application as the polymer must be semiconducting and photoactive. Polymers used for OSCs exhibit sp^2 -hybridization of carbon atoms thus allowing for photoactivity and charge transport. In OSCs, the polymer material is used as the p-type material. The most researched polymer material for OSC application is regioregular P3HT which is shown in Figure 2.1.

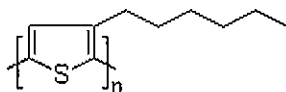


Figure 2.1: The monomer unit of P3HT [10].

P3HT is regioregular in the sense that carbon single and double bonds alternate due to p_z -orbital electrons in the sp^2 -hybridized carbon atoms forming π -bonds with neighboring p_z electrons. The end result is a linear chain of sp^2 -hybridized carbon atoms allowing for charge transport via molecular hopping [4].

2.2 Fullerene Material

A fullerene is a carbon ball typically made of either 60 or 70 carbon atoms, denoted by C_{60} and C_{70} respectively, for OSC applications. C_{60} has a spherical shape

whereas C_{70} has an oblong, ovular shape. Rather than using pure C_{60} or C_{70} fullerenes, OSCs use fullerene derivatives, materials with one or two side chains added to a C_{60} or C_{70} base to promote solubilization and to modify energy level. In OSCs, the fullerene derivative material is used as the n-type material. The most researched fullerene material for OSC application is $PC_{60}BM$ which is shown in Figure 2.2 [4, 11].

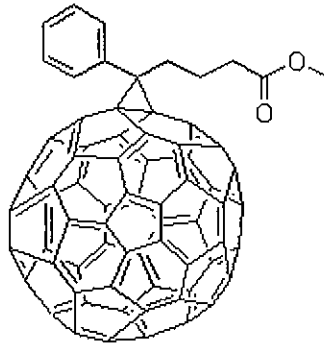


Figure 2.2: The molecular structure of $PC_{60}BM$ [12].

In OSCs, the V_{OC} is determined by the highest occupied molecular orbital (HOMO) energy of the polymer material and the lowest unoccupied molecular orbital (LUMO) energy of the fullerene material as shown in equation (1).

$$V_{OC} = \frac{1}{q} (|E^{POLYMER}(HOMO)| - |E^{FULLERENE}(LUMO)|) - V_{Loss} \quad (1)$$

where q is elementary charge, $E^{POLYMER}(HOMO)$ is the HOMO energy level of the polymer material, $E^{FULLERENE}(LUMO)$ is the LUMO energy level of the fullerene material, and V_{Loss} is a loss factor typically 0.3 V in OSCs. The HOMO and LUMO levels of organic materials are analogous to the valence and conduction bands of inorganic materials respectively [13]. As seen in the above equation, we can tune the

energy bands of the photoactive solution materials to increase the V_{OC} and thus, as we will see later, the PCE. If the same polymer is used, the V_{OC} is dependent on the fullerene material with fullerene derivatives with lower LUMO levels producing a higher V_{OC} . However, LUMO levels must still be properly aligned for sufficient exciton dissociation [11].

A desirable fullerene acceptor exhibits properly aligned LUMO levels, good solubility in organic solvents, high charge mobility, and good optical absorption [4, 11]. Table 2.1 summarizes various fullerene derivatives used in OSCs. The most commonly used fullerene, PC₆₀BM, exhibits an open circuit voltage of 0.60 V whereas other materials such as ICBA show open circuit voltages greater than 0.80 V. Typical fullerene derivatives used in OSC technology can be classified into one of seven categories as seen in Table 2.1: methanofullerenes, indenefullerenes, 1,4-Di(organo)fullerenes, fulleropyrrolidines, dihydronaphthyl fullerenes, penta(organo)fullerenes, or open cages fullerenes.

PC_{60/70}BM and other derivatives based off of PCBM such as Methano-PCBM and bis-PCBM fall under the methanofullerene category. These derivatives are fullerenes with a methanobridge with functional groups including aromatic rings or aliphatic chains attached. It has been reported that changing these functional groups in PCBM does not change electrochemical or optical properties but rather improves solubility up to about 80 mg/mL in chlorobenzene. Other reports indicate that electron mobility in these methanofullerenes can be increased as a response to improved morphology from the improved solubility. Energy level can also be changed by changing the number of π electrons in the fullerene [11].

Table 2.1: Several fullerene materials including LUMO level and exhibited V_{OC} [11].

Fullerene Derivative	Fullerene Category	LUMO (eV)	Reported V_{OC} (V)
PC ₆₀ BM	Methano-	-4.30	0.60
Bis-PCBM	Methano	-3.6	0.72
IC ₆₀ MA	Indene-	-3.86	0.58
IC ₇₀ MA	Indene-	-3.85	
IC ₆₀ BA	Indene-	-3.74	0.84
IC ₇₀ BA	Indene-	-3.72	0.84
SIMEF C ₆₀ (CH ₂ SiMe ₂ Ph) ₂	1,4-Di(organo)-	-3.74	0.75
1 C ₆₀ (1,2-di-CH ₂ - C ₆ H ₃ -4- CH ₂ OCOC ₆ H ₅)	Dihydronaphtyl	-4.11	0.65
Penta 4 C ₆₀ (C ₆ H ₄ OPh) ₅ Me	Penta(organo)-	-3.43	0.76
3	Open cage	-3.00	0.74

As the name suggests, indenefullerenes are fullerenes with indene side chains such as indene-C₆₀ monoadduct (ICMA) and ICBA. In ICMA, a singular indene side chain is used, hence the monoadduct term in its name. In ICBA, two indene side chains are used, hence the bisadduct term in its name. These fullerene derivatives show great promise as they increase V_{OC} while keeping J_{SC} and FF high [11]. As these derivatives, specifically IC₆₀BA, will be the main focus of the rest of this paper, the molecular structure of IC₆₀BA is given in Figure 2.3.

1,4-Di(organo)fullerenes have functional groups added onto the 1,4-position of the fullerene. As with the previous fullerenes, changing these functional groups allows for the changing of solubility and energy level. The promise of these materials lies in their much higher absorption extinction coefficient [11].

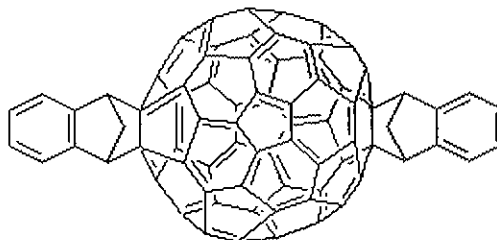


Figure 2.3: Molecular structure of ICBA indenefullerene [14].

Fulleropyrrolidines use a sarcosine amino acid to attach the functional groups. These fullerenes exhibit strong absorption of visible light in the 500-600 nm range, not typical of fullerenes such as PCBM. However, devices utilizing these materials exhibit lower PCEs due to inefficient charge separation[11].

Dihydronaphthyl fullerenes are processed by reacting C₆₀ with ortho-dimethinequinine. Devices fabricated with these materials show slightly enhanced open circuit voltages [11].

Penta(organo)fullerenes are processed by adding organocopper reagent to C₆₀. These fullerenes are “stackable” in the sense that they are able to assemble head-to-tail. Because of this stacking, a homogenous P3HT:fullerene layer is difficult to obtain resulting in low current. Additionally, the LUMO level of these materials, ≈ 3.00 eV, might be too high-lying hindering charge separation. Thus, devices utilizing penta(organo)fullerenes exhibit lower PCEs than standard P3HT:PCBM devices [11].

Open caged fullerenes are, as the name states, a fullerene with removed bonds forming a “hole” such that the fullerene ball resembles an open cage. Organic dyes can thus be used to tune optical absorption properties. Devices fabricated with open caged fullerenes exhibit PCEs on par with conventional P3HT:PCBM devices [11].

This thesis will focus on P3HT:ICBA solar cells as they show the highest potential V_{OC} [11]. The actual chemical processing of the above fullerene materials is outside of the scope of this thesis; as such, I will only focus on their use in photovoltaic devices.

2.3 Device Architecture

First generation OSC devices used a single p-type organic polymer sandwiched between electrodes of different work functions. This difference in work function provides for an electric field which is able to dissociate excitons, coulombically bound electron-hole pairs, into free electrons and holes. The exciton dissociation energy is high in OSCs; thus, special care must be taken when selecting electrodes. This implementation of electrodes with different work functions is still in use in modern OSC architectures to allow for efficient exciton dissociation [4].

The next generation of OSC devices employed a bilayer heterojunction architecture in which donor polymer and acceptor fullerene are stacked one on top of the other such that a single interface is formed similar to a typical semiconductor PN junction. This evolution step in OSC technology allowed for less recombination as electrons and holes are spatially separated in the fullerene and polymer respectively. However, issues arise from recombination due to the low exciton diffusion length in these organic materials requiring extremely thin layers resulting in poor absorption, a problem the next generation of OSC devices seeks to solve [4].

The current generation of OSC devices uses a so-called bulk heterojunction (BHJ). In the BHJ, polymer and fullerene are mixed together resulting in an increased

amount of donor:acceptor interface within the exciton diffusion length. Doing so, absorption is increased as thicker layers can be used. A huge problem arising in this architecture type is recombination traps due to insufficient pathways to respective electrodes. Thus, nanoscale morphology of the BHJ layer is of extreme importance. This BHJ architecture provides a good balance between ease of processing and performance [4].

The next architecture researchers hope to realize the nanostructured architecture. By using templates, nanoscale control of the morphology allows for highly ordered vertical arrays of P3HT and PCBM. Such a highly ordered architecture would eliminate the recombination problems inherent to the BHJ as a result of trapping islands. Currently, research lies in attaining highly controlled nanofabrication methods in line with the processing goals of organics [15]. Figure 2.4 shows the above four architectures.

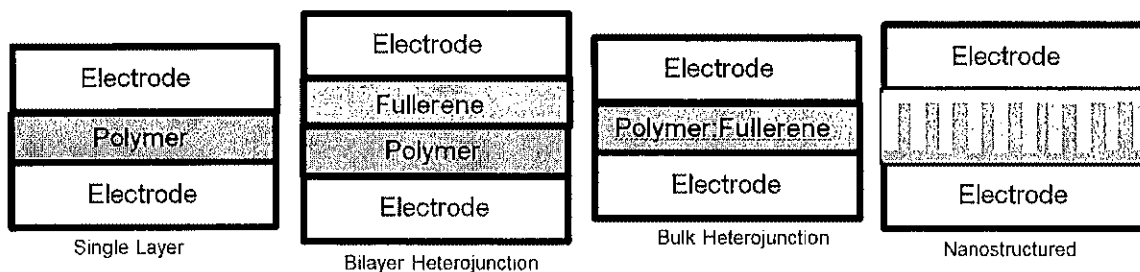


Figure 2.4: The evolution of OSC architectures.

The energy diagram and device structure for the P3HT:ICBA solar cells of interest to this thesis are given in Figure 2.5. The energy levels are nicely aligned to allow for dissociated electrons at the P3HT:IC₆₀BA interface to be extracted to the Al electrode

and for dissociated holes to be extracted at the ITO electrode.

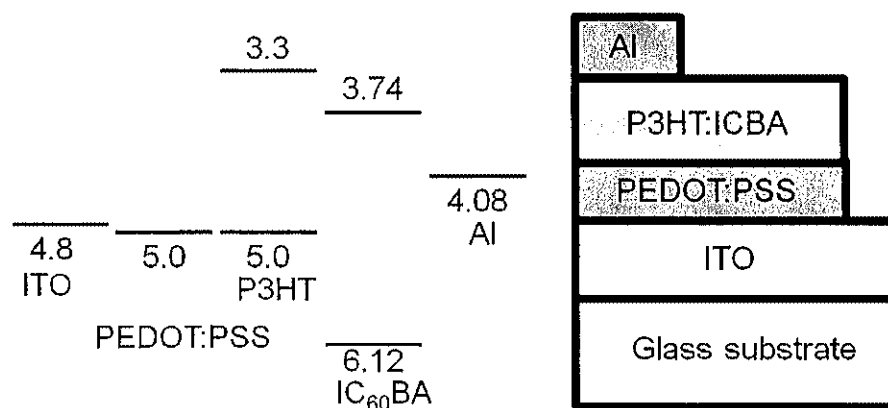


Figure 2.5: Energy band diagram of the P3HT:IC₆₀BA solar cell of interest on the left. Energy values are given in eV and are from [4, 11]. Experimental device architecture not to scale on the right.

2.4 Operation

Organic solar cells operate in four steps: photon absorption and exciton generation, exciton diffusion, exciton dissociation, and charge extraction. In the first step, photons with sufficient energy greater than the band gap of the polymer are absorbed by the photoactive polymer generating excitons. Next, these excitons must diffuse to donor:acceptor interfaces. At these interfaces, the excitons dissociate due to the built in electric field which generates free electrons and holes. Finally, these free carriers must be extracted at the electrodes, generating current [2, 4, 5]. This operation is shown pictorially in Figure 2.6.

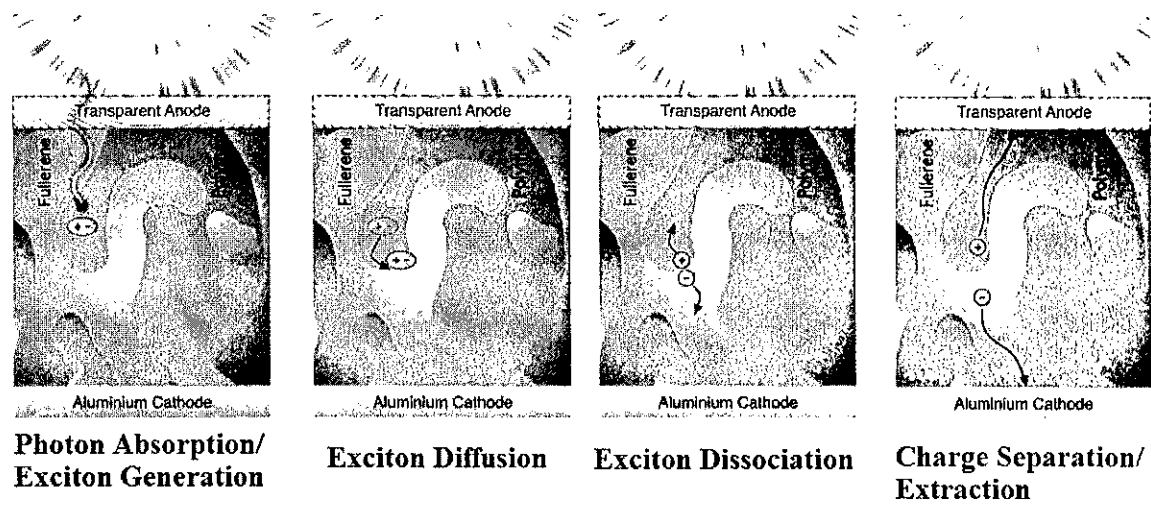


Figure 2.6: Operation of an OSC [16].

CHAPTER 3

FABRICATION PROCESS AND CHARACTERIZATION METHODS

3.1 Organic Solar Cell Fabrication Process

ITO coated glass slides with resistance of $10 \Omega/\square$ are purchased from NanoCS. The as-received 1 inch by 3 inch slides are cut into 1 inch by 1 inch squares by scoring the backside multiple times using a diamond scribe. Silicone polyimide tape of width 0.25 inch is used to mask off two ITO anode areas. The masked slides are immersed in a heated (60 °C) acidic etching solution composed of 5% HNO_3 , 20% HCl , and 75% deionized water. Complete etching is verified using a multimeter; then, tape residue is removed by wiping the substrates with cotton wipes and acetone. The resulting 1 inch by 1 inch ITO substrates are cleaned to remove contaminants and oils by subsequent ultrasonication in heated (60 °C) 3% Mucosol detergent solution, deionized water, isopropyl alcohol, and acetone. The cleaned glass slides are blown dry with N_2 and are further dried by baking on a hot plate at 100 °C for at least 12 hours in a glove box filled with industrial grade nitrogen.

Photoactive layer solutions are made prior to fabrication due to the long stirring times required. P3HT:PCBM active layer solution is made by measuring 30 mg of P3HT and 24 mg of PCBM and dissolving the mixture in 2 mL of chlorobenzene (CB) in a glass vial. A magnetic spin bar is also placed in the vial. The resulting solution is stirred at 200 rpm and heated to 60 °C in a glove box for 15 hours. For this thesis work, several P3HT:ICBA solutions listed in Table 3.1 were made for further studies.

Table 3.1: P3HT:ICBA solution preparation parameters.

P3HT:ICBA Solutions Prepared				
	Solvent	Additive	Sonication	Stirring Conditions
1	2 mL DCB	None	None	a
2	2 mL DCB	None	1 hour	b
3	2 mL CB	None	1 hour	b
4	1 mL DCB : 1 mL CB	None	1 hour	b
5	1.2 mL DCB : 0.8 mL CB	None	1 hour	b
6	2 mL DCB	3% w/v octanedithiol	1 hour	b
7	2 mL DCB	None	1 hour	c
Stirring Condition Definitions				
a	Stir 15 hours at 200 rpm and 60 °C			
b	Stir 5 hours at 200 rpm and 100 °C; Stir 15 hours at 200 rpm and room temperature			
c	Stir P3HT and ICBA separately and subject to Condition b			
	Note: Weight concentration is 25 mg P3HT : 25 mg ICBA for all solutions			

P3HT:ICBA solution is made by measuring 25 mg of P3HT and 25 mg of ICBA and dissolving in either dichlorobenzene (DCB), CB, or a mixture of both solvents as in Solutions 4 and 5 in a glass vial. Additionally, the solvent additive 1,8-octanedithiol (ODT) may be added to the solution in a 3% weight/volume (w/v) concentration as in Solution 6. The solutions may then be ultrasonicated for 1 hour as in Solutions 2-7. For ultrasonicated solutions, glass vials are packed in an air tight container filled with nitrogen in the glove box to prevent degradation. The solutions are then subjected to one of three stirring conditions in a glove box: stirring for 15 hours at 200 rpm and 60 °C as in Solution 1, stirring for 5 hours at 200 rpm and 100 °C and then stirring for 15 hours at 200 rpm and room temperature as in Solution 2, and stirring the P3HT and ICBA separately for 5 hours at 200 rpm and 100 °C and then stirring for 15 hours at 200 rpm and room temperature as in Solution 7. For Solution 7, after stirring for 15 hours the

P3HT and ICBA solutions are mixed together in one vial to produce a P3HT:ICBA blend solution.

For both P3HT:PCBM and P3HT:ICBA devices, Clevios P VP AI 4083 poly(3,4-ethylenedioxythiophene) poly(styrenesulfonate) (PEDOT:PSS) purchased from Heraeus is spin cast onto the dried ITO substrates in air at a speed of 3000 rpm with 500 rpm/s acceleration for 3 minutes. The PEDOT:PSS layer is then baked to remove the water the PEDOT:PSS is dissolved in by placing on a hotplate at 100 °C for 15 minutes in air. Samples are then transferred to a glove box.

For P3HT:PCBM devices, the P3HT:PCBM solution is spin cast onto the substrate at a speed of 1250 rpm with 500 rpm/s acceleration for 60 seconds. P3HT:ICBA solution is spin cast at a speed of 600 rpm with 500 rpm/s acceleration for 60 seconds. Resulting P3HT:PCBM or P3HT:ICBA films are allowed to dry in the glove box antechamber under vacuum for 20 minutes. Samples are then taken out of the glove box to clean off the ITO anode area and backside with trichloroethylene and q-tips.

The samples are then transferred to an electron-beam evaporator chamber for aluminum cathode deposition. Vacuum on the order of 10^{-7} torr is attained with a mechanical roughing pump and a diffusion pump. After sufficient pump down time, 80 nm of aluminum is deposited at an average rate of about 1.3 Å/s through a shadow mask resulting in 8 individual devices with an area of 0.11 cm² on a single ITO substrate. After waiting 20 minutes for the substrates to cool, the vacuum is broken and the substrates are transferred back into the glove box for post-annealing at 150 °C for 10 minutes. The resulting solar cells are then ready for characterization.

3.2 Electrical Characterization

The produced OSCs are characterized electrically with JV plots. The JV plots are obtained by illuminating the solar cells using a Newport Oriel solar illuminator in constant power mode (100 W) fitted with an AM 1.5 G filter to ensure characterization adheres to National Renewable Energy Laboratory standards (1000 W/m², 25 °C, AM 1.5 G). A Newport reference solar cell and meter is used to measure sun irradiance and temperature. Upon verifying correct irradiance (1 sun) and temperature (25 °C), A computer interfaced Keithley 2400 SourceMeter is used to apply voltage in increments and to measure current at those increments resulting in a current-voltage (IV) plot. For reporting purposes a JV plot is calculated from the obtained IV plot by dividing current by the device active area, 0.11 cm² in this work.

From a JV plot we can obtain much information including open circuit voltage (V_{OC}), short circuit current density (J_{SC}), maximum power point (MPP), fill factor (FF), and power conversion efficiency (PCE). V_{OC} is the voltage where J is zero, and J_{SC} is the current density where V is zero. The MPP corresponds to the point at which the produced power is greatest. The voltage and current density at this point are referred to as V_{max} and J_{max} respectively.

The FF is a measure of the plot's shape and is calculated as the ratio of the maximum power to the product of V_{oc} and J_{sc} as in equation (2).

$$FF = \frac{P_{max}}{V_{oc}J_{sc}} = \frac{V_{max}J_{max}}{V_{oc}J_{sc}} \quad (2)$$

The PCE, perhaps the most important solar cell parameter, is the ratio of the maximum produced power density to the input power density received from illumination as in equation (3).

$$PCE = \frac{FF \times V_{oc} \times J_{sc}}{P_{in}} \quad (3)$$

A more detailed discussion of the physical meaning of the above parameters will be given in the following chapter.

To obtain a deeper understanding of device physics, analyzing an equivalent circuit model can be useful in determining series (R_s) and shunt resistances (R_{sh}), diode ideality factor (n), and diode reverse saturation current density (J_0). By fitting an obtained JV plot to equation (4) below derived from an equivalent circuit model, we can extract the four previously mentioned parameters.

$$J = \frac{W\left(\frac{\beta}{n} \frac{R_s R_{sh} J_0}{R_s + R_{sh}} \exp\left[\frac{\beta}{n} \frac{R_{sh}}{R_s + R_{sh}} (V + R_s J_0 + R_s J_{ph})\right]\right)}{\frac{\beta}{n} R_s} - \frac{R_{sh}}{R_s + R_{sh}} \left(J_0 + J_{ph} - \frac{V}{R_{sh}}\right) \quad (4)$$

In equation (4), J_{ph} is photocurrent density, β is inverse thermal voltage, and V is the applied voltage. W is the Lambert W-function $W(x)$ which is used in order to find an analytic solution to the diode model with resistances [17]. A more detailed discussion of the physical meaning of the extracted parameters will be given in the following chapter.

3.3 Physical Characterization

To obtain physical properties of the spin cast thin films, atomic force microscopy (AFM), X-ray diffraction (XRD), and high-resolution digital imaging were performed. To prepare samples for the above characterization techniques, plain glass slides were cut into 1 inch by 1 inch squares. The substrates were cleaned using the same cleaning procedure discussed previously. The photoactive layer solution of interest was then spin cast onto the cleaned glass substrate in the glove box. The thin film was allowed to dry for 20 minutes under vacuum in the antechamber. Finally, the sample was ready for

characterization. All samples were characterized using a Digital Instruments Veeco Dimension 3100 AFM in tapping mode. System parameters used are as follows: a 1.00 μm scan size, a 1.00 Hz scan rate, and 512 samples/line. For XRD, a Rigaku Miniflex II system was used to measure diffraction intensity between 2θ values of 3° and 8° . A scan speed of $2^\circ/\text{min}$ was used with a sampling width of 0.2° . For high-resolution digital imaging, a HIROX KH-7700 digital-video microscopy system outfitted with a x35 MXG-2500REZ lens was used to capture high resolution images of the studied thin films.

3.4 Optical Characterization

The most important optical property of the studied OSCs is absorption in the ultraviolet-visible range. As discussed in Chapter 2, photons must be absorbed in order to produce charge carriers; as such, an increased number of absorbed photons is beneficial to OSC performance. The number of absorbed photons can be measured using UV-Vis spectroscopy which measures absorption in absorbance units (AU) as a function of wavelength. To prepare samples for UV-Vis spectroscopy, the procedure mentioned in the previous section was used. A UV-Vis spectrum of the sample was then obtained using a PerkinElmer Lambda 45 with a slit width of 1 nm and a scanning speed of 480 nm/min.

CHAPTER 4

RESULTS, ANALYSIS, AND DISCUSSION

4.1 Electrical Properties

Initially, P3HT:PC₆₀BM and P3HT:IC₆₀BA devices were fabricated simultaneously to obtain base comparison results as seen in Figure 4.1 and Table 4.1. Interestingly, the IC₆₀BA device showed an open circuit voltage and a short circuit current much lower than that of the PC₆₀BM device but a higher FF. These first IC₆₀BA devices showed high nonuniformity which may have caused an extreme number of recombination sites in the active layer resulting in the low V_{OC} and J_{SC}.

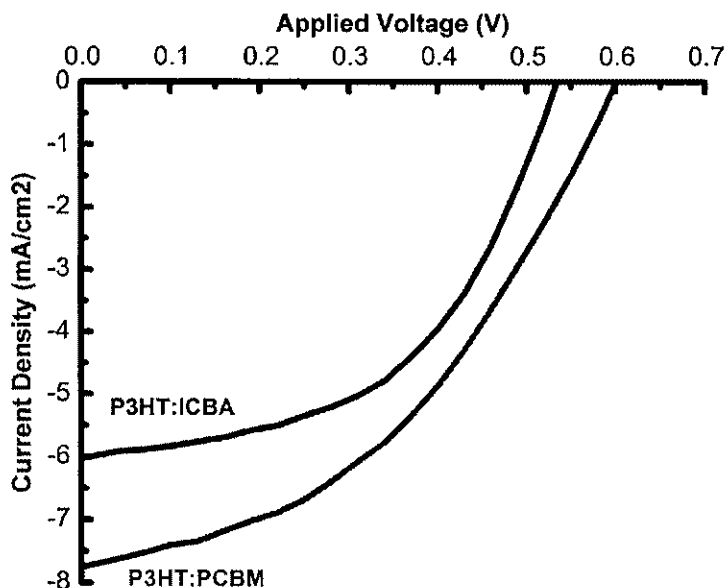


Figure 4.1: An initial comparison of the JV plots of IC₆₀BA and PC₆₀BM photovoltaic devices.

Table 4.1: Photovoltaic properties of the devices shown in Figure 4.1.

Photoactive Solution	V_{OC} (V)	J_{SC} (mA/cm²)	FF	PCE (%)
P3HT:ICBA	0.5339	6.0208	0.5033	1.6176
P3HT:PCBM	0.6008	7.7596	0.4208	1.9615

After repeating the above experiment several times with the same general trend, it is found that the high purity material exhibits poor solubility in common organic solvents and thus requires additional steps when mixing the active layer solution. Therefore, it is necessary to revise the active layer solution mixing step to include ultrasonication for 1 hour prior to stirring at 200 rpm and heating to 100 °C for 5 hours followed by stirring at 200 rpm at room temperature overnight. Additionally, another solution was made in which P3HT and ICBA were sonicated and stirred separately prior to mixing together for spin casting. The resulting thin films exhibited a more uniform film upon visual inspection; however, it is found that clumps of ICBA material still exist in the thin film as will be seen in more detail later. The resulting JV curve is seen in Figure 4.2 with a summary of photovoltaic properties in Table 4.2. As seen in the figure and table, V_{OC} increased to values greater than 0.6 V but was still much lower than those found in literature [11].

Comparing the sonication treatments, we see that sonication leads to increased V_{OC} and slightly increased J_{SC}. Since V_{OC} is an indication of device recombination [1], it is plausible that sonication improves solubility and thus device nanomorphology to decrease recombination trapping sites. This plausibility will be discussed later in terms of physical and optical properties. Interestingly, the device which used a photoactive solution stirred separately exhibited the highest V_{OC} but the lowest J_{SC}. This low J_{SC}

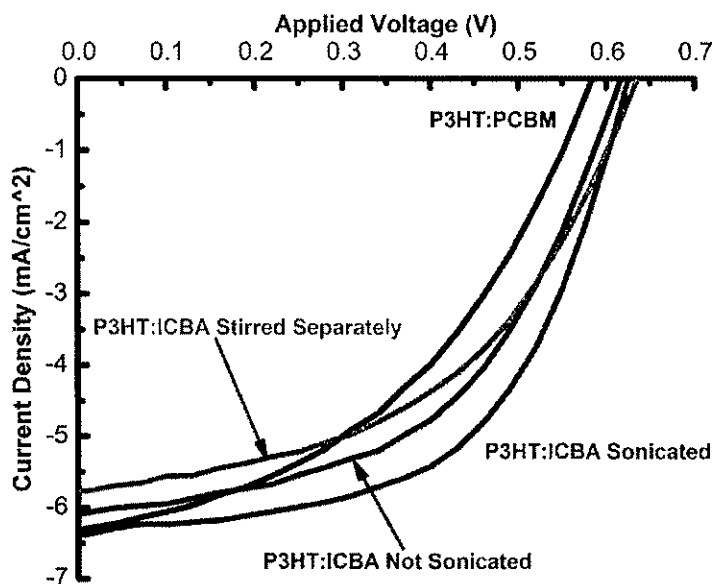


Figure 4.2: JV curves comparing sonication treatments of P3HT:ICBA devices.

Table 4.2: Photovoltaic properties with different sonication treatments.

Sonication Treatment	V_{OC} (V)	J_{SC} (mA/cm ²)	FF	PCE (%)
P3HT:PCBM	0.584	6.315	0.433	1.599
P3HT:ICBA Sonicated	0.625	6.380	0.551	2.200
P3HT:ICBA Not Sonicated	0.617	6.093	0.505	1.899
P3HT:ICBA Stirred Separately	0.636	5.767	0.480	1.759

might be attributed to optical losses due to losing some of the polymer material or solvent when combining the separate solutions. This will be discussed in the following section.

Further inspection of the JV curves in Figure 4.2 reveals that the sonicated solution not stirred separately exhibits the best photovoltaic performance due to high V_{OC} and J_{SC} .

The higher J_{SC} might be attributed electrically to a lower series resistance as estimated by the inverse slope at V_{OC} . This higher J_{SC} will be further discussed in terms of improved

device nanomorphology and optical absorbance shortly.

Further literature review indicates that ICBA exhibits poor solubility in dichlorobenzene and that using a mixed solvent of dichlorobenzene (DCB) and chlorobenzene (CB) may improve the solubility resulting in improvement of photovoltaic properties [18]. Thus, an experiment was conducted to compare the photovoltaic performance of devices using P3HT:ICBA dissolved in four different solvent mixtures: 2 mL DCB, 1.2 mL DCB : 0.8 mL CB, 1 mL DCB : 1 mL CB, 2 mL CB. The results of this experiment are seen in Figure 4.3 and Table 4.3. Of the four solutions, the pure CB solution showed the lowest V_{OC} and J_{SC} resulting in the lowest PCE. The pure DCB solution showed intermediate V_{OC} , J_{SC} , and therefore PCE while the mixed solutions showed improvements in photovoltaic properties with the 1 mL DCB : 1 mL CB solvent exhibiting the highest J_{SC} and PCE. Increasing the amount of CB in the mixed solution resulted in increased J_{SC} and PCE. Differences in J_{SC} might be attributed to differences in optical absorption, recombination due to nanomorphology and trapping sites [1, 19]. The first two mentioned possibilities will be described later in this thesis while different recombination processes are studied now.

As discussed in Chapter 3, fitting to equation 4 was done to extract ideality factor (n), and reverse saturation current density (J_0) for the mixed solvent data points. The extracted results are given in Table 4.4. Diode reverse saturation current density (J_0) can provide valuable insight into the amount of recombination and the density of interface defect states of organic solar cells [1, 19]. Comparing the J_0 values, we see that the pure DCB and pure CB solutions exhibit higher values than the mixed solutions. This suggests that devices fabricated with the mixed solvents exhibit less recombination than the other

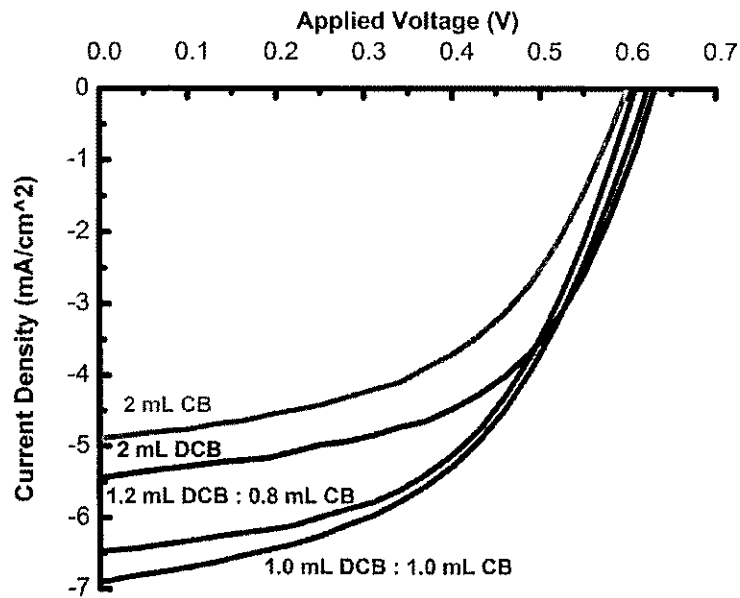


Figure 4.3: JV curves for the mixed solvent experiment

Table 4.3: Photovoltaic properties for mixed solvent active solutions.

Mixed Solvent Ratio	V_{OC} (V)	J_{SC} (mA/cm ²)	FF	PCE (%)
2 mL DCB	0.631	5.436	0.537	1.841
1.2 DCB : 0.8 CB	0.609	6.476	0.515	2.032
1 DCB : 1 CB	0.623	6.893	0.492	2.109
2 mL CB	0.600	4.893	0.506	1.484

Table 4.4: Extracted solar cell parameters for the mixed solvent experiment.

Solution	n	J_0 (mA/cm ²)
2 mL DCB	3.0006	1.7101×10^{-4}
1.2 DCB: 0.8 CB	2.9577	6.7667×10^{-5}
1 DCB: 1 CB	2.8941	6.3738×10^{-5}
2 mL CB	3.3019	8.6119×10^{-4}

two solutions, perhaps slightly contributing to the higher short circuits. Of the four devices, the 1 mL DCB : 1 mL CB solvent showed the lowest J_0 , a trait characteristic of high performing solar cells. Furthermore, the reverse saturation current is related to the density of interface defect states by:

$$J_0 = qAD_{it}kT\omega_0e^{-E_b/kT} \quad (5)$$

where q is elementary charge, A is active area factor, D_{it} is the density of interface states per unit interfacial area per electron volt, E_b is relevant excitation energy, k is the Boltzmann constant, T is temperature, and ω_0 is rate prefactor [20]. We are mainly concerned with the direct relationship between J_0 and D_{it} . Thus, it is found that the pure DCB and CB solutions exhibit a higher density of interface defects which should contribute to more recombination and slightly decreased J_{SC} .

Diode ideality factor can reveal much about the transport and recombination mechanics of the organic solar cell. Interestingly, the diode ideality factors for all four devices were high compared to the typical ideality factors (n) of silicon solar cells which exhibit n between 1 and 2 [1]. For typical n close to 1, bimolecular radiative band-to-band recombination dominates [21]. Diode ideality factor closer to 2 indicates Shockley-Read-Hall recombination through a single defect or trap level [22]. The above solar cells, however, show ideality factors greater than 2 suggesting alternative recombination mechanics. Multi-level recombination is thus a possibility [19]. Again, we see that the mixed solvents show slightly lower n values suggesting a lower amount of multi-level recombination. The lowest n is seen again for the 1 mL DCB : 1 mL CB solvent contributing further to its high PCE.

Additionally, literature indicates that 1-8-octanedithiol (ODT) can be used to

improve solubility [23]. As such, an experiment was conducted to study the effects of ODT on P3HT:ICBA solar cells. The results of this experiment are seen in Figure 4.4 and Table 4.5. Using ODT as a solvent additive increases both V_{OC} and J_{SC} contributing to a higher PCE. Visual inspection of the spin cast thin films shows improvement of film uniformity when using ODT to be observed in more detail later in the thesis.

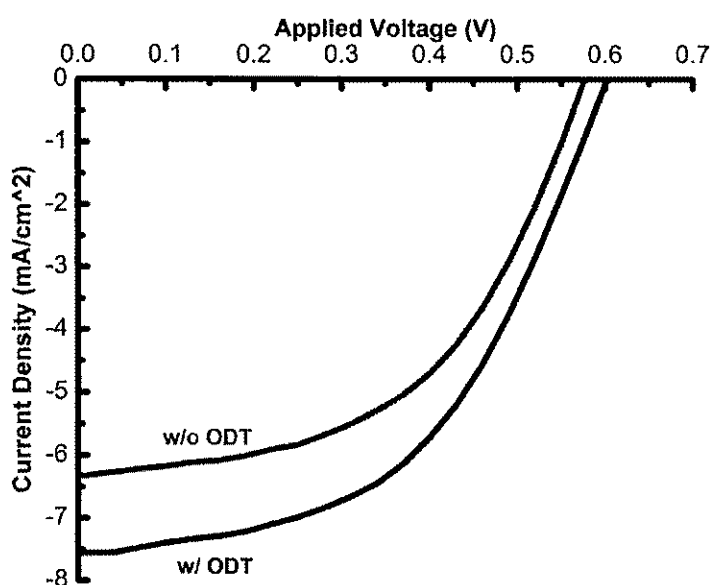


Figure 4.4: JV curves for the solvent additive experiment.

Table 4.5: Photovoltaic properties for the solvent additive experiment.

Solution	V_{OC} (V)	J_{SC} (mA/cm ²)	FF	PCE (%)
No ODT	0.577	6.327	0.510	1.862
3% w/v ODT	0.602	7.558	0.494	2.250

4.2 Physical Properties

AFM imaging and analysis correlated surface roughness with thin film uniformity. Additionally, HIROX imaging was also qualitatively compared with the studied thin films. Similar to the JV curves, we can make comparisons between the experiments done for this thesis. First, we observe thin films for the sonication experiment as shown in Figure 4.5. Of the ICBA thin films, the solution which was sonicated with 3% w/v ODT shows the smoothest and most uniform AFM scan validating visual inspections. The scan and image shows that using ODT as a solvent additive does promote solubility as the scan is more uniform and less rough as compared to the scans without the additive, perhaps contributing slightly to the increase in device efficiency as seen previously. In comparison to the solution sonicated with both polymer and fullerene together, the solution which was sonicated and stirred separately showed a smoother and more uniform surface; however, this solution also showed the lowest PCE due to high R_s and low J_{SC} as discussed previously. Furthermore, the sonicated solution has a lower RMS surface roughness than the non-sonicated solution providing further proof that sonication improves solubility. This observation is in agreement with the HIROX images which show a higher density of clusters in the non-sonicated thin film which might reduce device efficiency.

We now compare the mixed solvent thin films in Figure 4.6. The thin film cast from pure CB showed the smoothest and most uniform AFM scan and a clean HIROX image with no clusters verifying visual inspections which leads one to believe that a device fabricated using this solution would perform better, but for reasons discussed previously it does not. Increasing the amount of DCB in a mixed solvent also increases

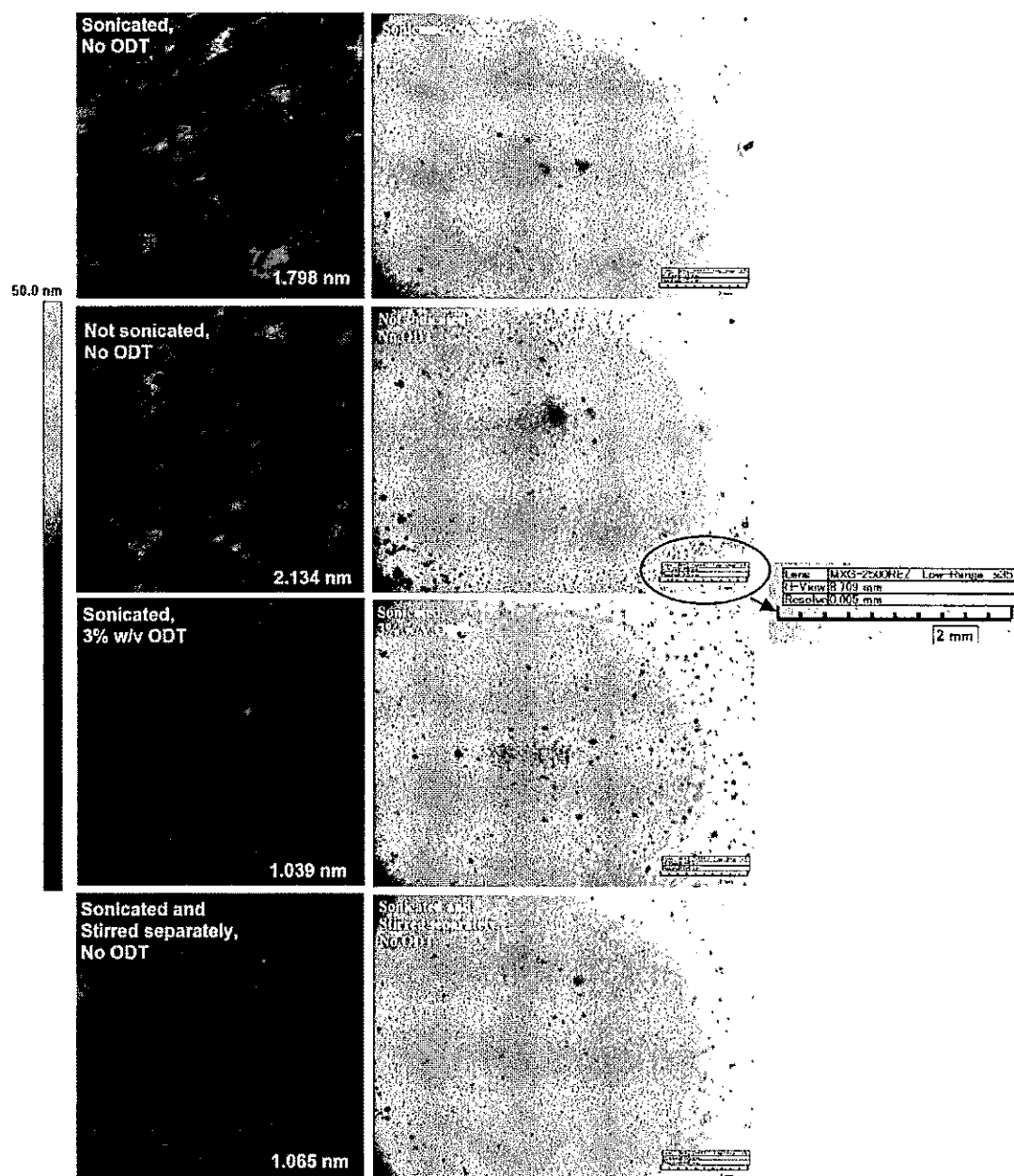


Figure 4.5: 1 μm x 1 μm AFM scans of the studied thin films for the sonication treatment experiment on the left. RMS roughness for the thin films is shown in the bottom right of the scans. HIROX images on the right.

the surface roughness. Moreover, the HIROX images show a similar pattern; increasing the amount of DCB increases the amount and size of clusters found. From the AFM scans

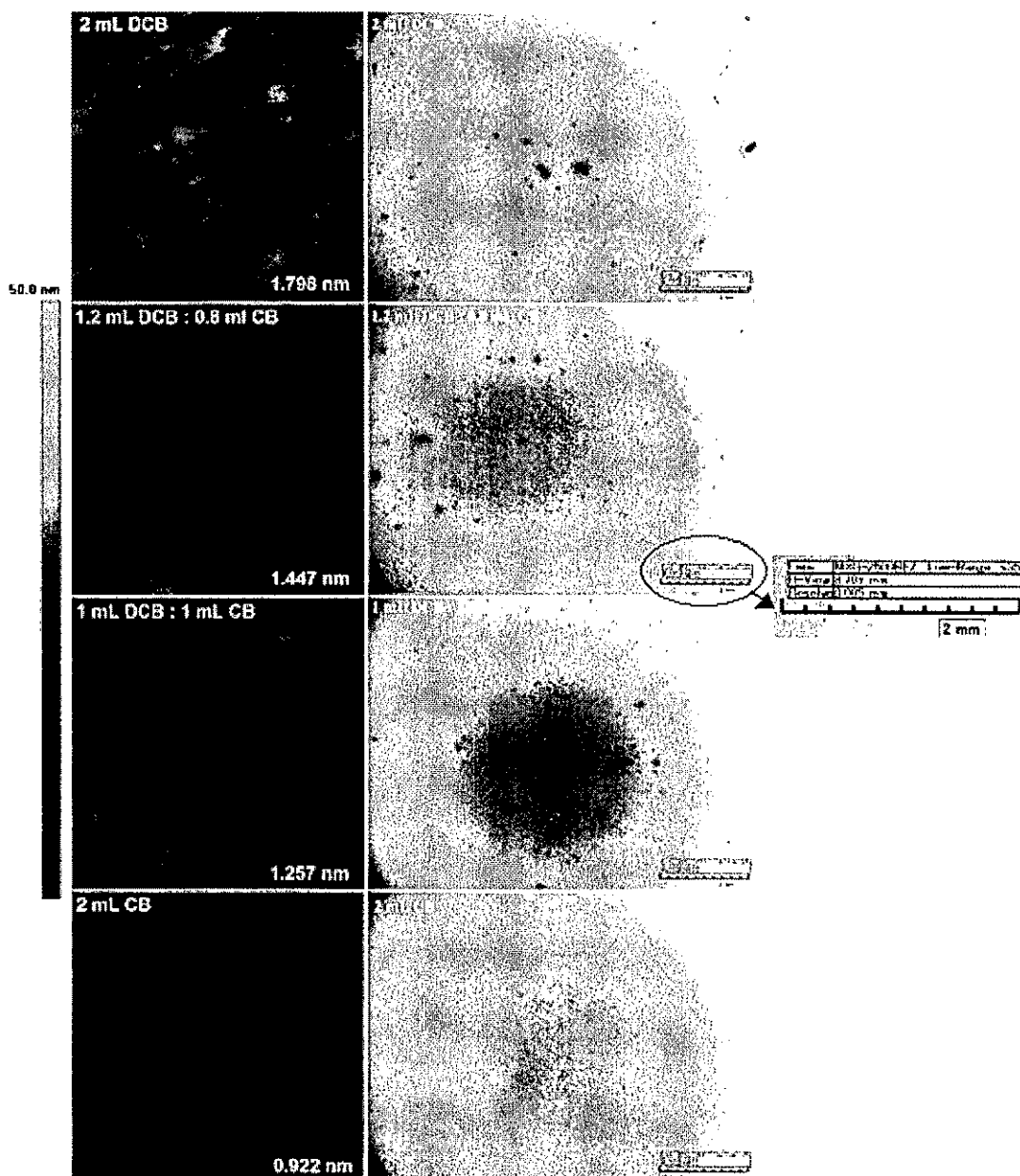


Figure 4.6: $1\ \mu\text{m} \times 1\ \mu\text{m}$ AFM scans of the studied thin films for the mixed solvent experiment on the left. RMS roughness for the thin films is shown in the bottom right of the scans. HIROX images on the right

and HIROX images, it is possible to conclude that CB enhances solubility, but a mixed solvent rather than a pure CB solvent is preferred for reasons discussed previously.

Further analysis of thin film structure and morphology was done with XRD. XRD

peak information is useful in comparing molecular ordering of thin films [24]. XRD spectra of the sonication experiment thin films are shown in Figure 4.6, and peak information is given in Table 4.6. Figure 4.6 shows similarly shaped spectra with peaks around $2\theta = 5.3^\circ$, but the peaks vary in height and width. The thin film cast from the

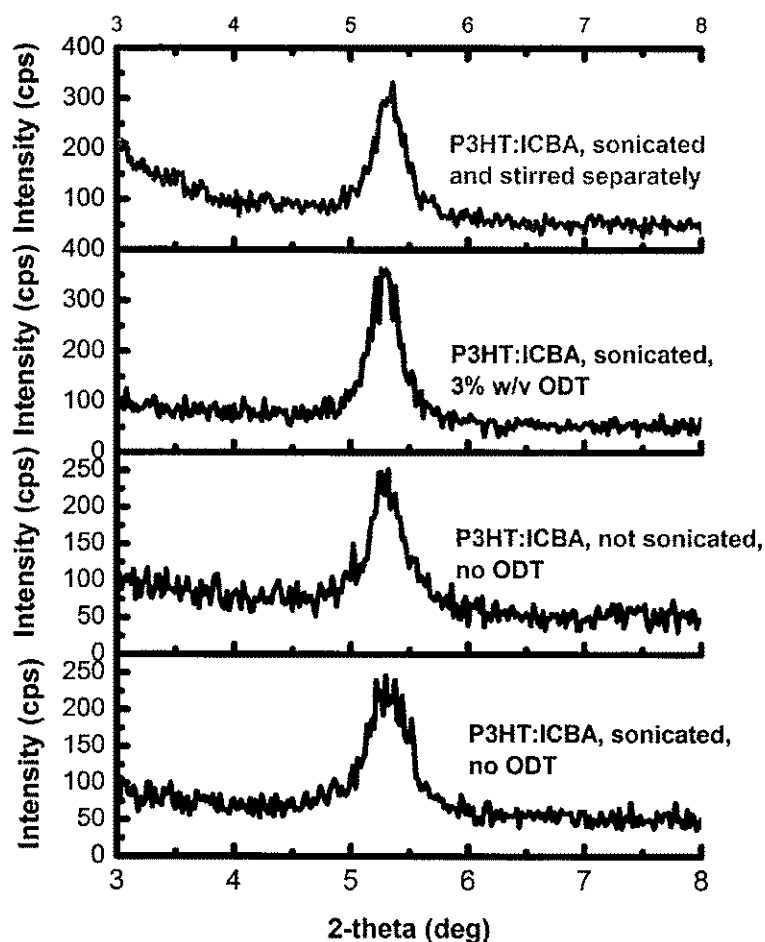


Figure 4.7: XRD spectra of the sonication experiment.

Table 4.6: XRD peak information of the sonication experiment.

Sonication Treatment	d(ang.)	2-theta(deg)	Height(cps)	FWHM(deg)	Int. I(cps deg)
Sonicated, No ODT	16.723	5.280	111.670	0.402	60.310
Not Sonicated, No ODT	16.766	5.267	110.460	0.359	53.820
Sonicated, 3% w/v ODT	16.665	5.299	194.230	0.296	80.030
Sonicated and Stirred Separately	16.559	5.332	153.820	0.305	62.340

solvent with the ODT additive exhibited the sharpest, highest intensity peak with the largest peak area. This peak, in addition to the AFM scan seen earlier, points to an improved nanomorphology due to higher molecular ordering brought about by increased P3HT aggregation [23]. As compared to the sonicated solution, the solution which received no sonication treatment exhibits a slightly smaller peak with less total peak area suggesting a decline in molecular ordering. This decreased molecular ordering might further contribute to the decrease in J_{SC} seen previously as a less ordered BHJ exhibit lower charge carrier mobilities.

Figure 4.7 and Table 4.7 show XRD spectra and peak information of the mixed solvent experiment. The pure CB solvent produced the lowest height XRD peak of all studied thin films despite a rather smooth surface. Despite a uniform thin film and good solubility as seen in AFM scans and HIROX images, the molecular ordering is disarrayed, resulting in the observed decreased J_{SC} . Using mixed solvents improves the intensity of the XRD peaks compared to using a pure CB solvent; the 1 mL DCB : 1 mL CB solvent shows marked improvements in terms of peak height and area. Despite a slightly lower peak intensity and area as compared to the device made from a pure DCB

solvent, the device made from this mixed solvent exhibits superior photovoltaic properties. It seems that this device exhibits a good balance of electrical properties in terms of n and J_0 discussed previously and physical properties in terms of uniformity and nanomorphology. Optical properties of these devices will be studied shortly.

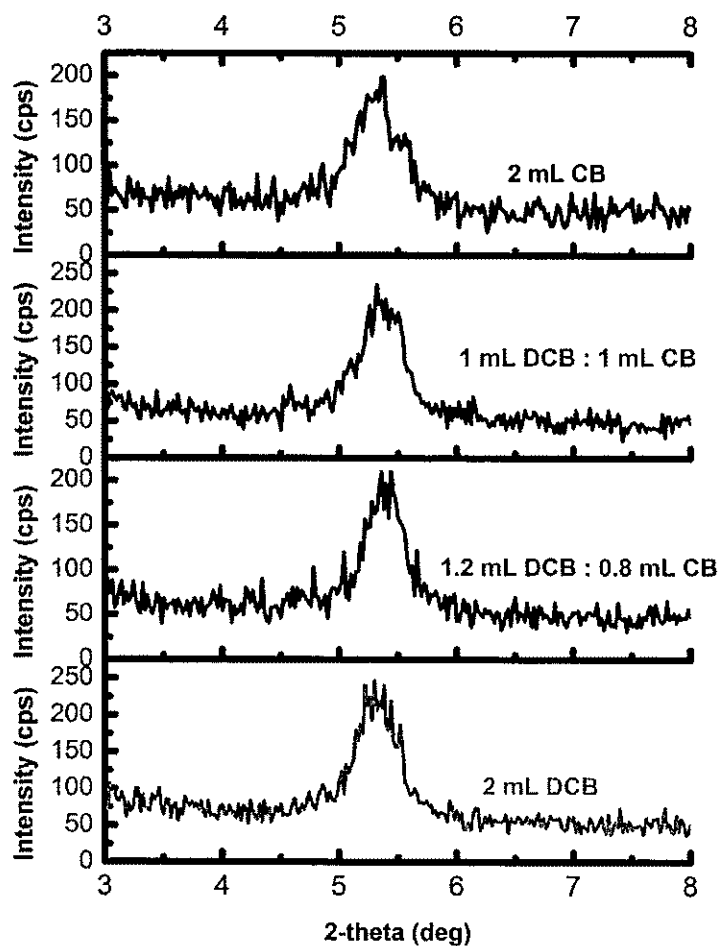


Figure 4.8: XRD spectra of the mixed solvent experiment.

Table 4.7: XRD peak information of the mixed solvent experiment.

Mixed Solvent Ratio	d(ang.)	2-theta(deg)	Height(cps)	FWHM(deg)	Int. I(cps deg)
2 mL DCB	16.723	5.280	111.670	0.402	60.310
1.2 DCB : 0.8 CB	16.400	5.384	94.940	0.369	49.830
1 DCB : 1 CB	16.271	5.427	102.270	0.441	55.900
2 mL CB	16.720	5.281	79.310	0.481	45.760

4.3 Optical Properties

Optical characterization was done with UV-Vis absorption measurements. The obtained spectra for the sonication experiment are shown in Figure 4.7, and peak information and total area under the curves are given in Table 4.6. Absorption in the UV range lower than 400 nm for P3HT:IC₆₀BA devices can be attributed to the presence of IC₆₀BA whereas peaks in the visible region of the spectrum can be attributed to the P3HT material [25, 26].

As seen in the figure and table, the P3HT:ICBA solution which was sonicated and contained no ODT exhibits the highest peak intensity and largest total absorption as determined by the area under the curve. This solution also showed the highest J_{SC} and PCE as seen earlier in the chapter. Interestingly, the solution which was sonicated and stirred separately showed the lowest peak intensity and total absorption. As a result, this solution showed the lowest J_{SC} and PCE of the ICBA solutions. Additionally, the solution which was sonicated and stirred separately shows a blueshifted peak indicating decreased P3HT polymer conjugation length [28]. This decrease in conjugation length results in the observed decrease in J_{SC} as charge mobility is hindered due to lower charge carrier transport by molecular hopping [28]. The two absorption shoulders for the thin films at about 530 nm and 600 nm can provide some insight into the molecular ordering of the

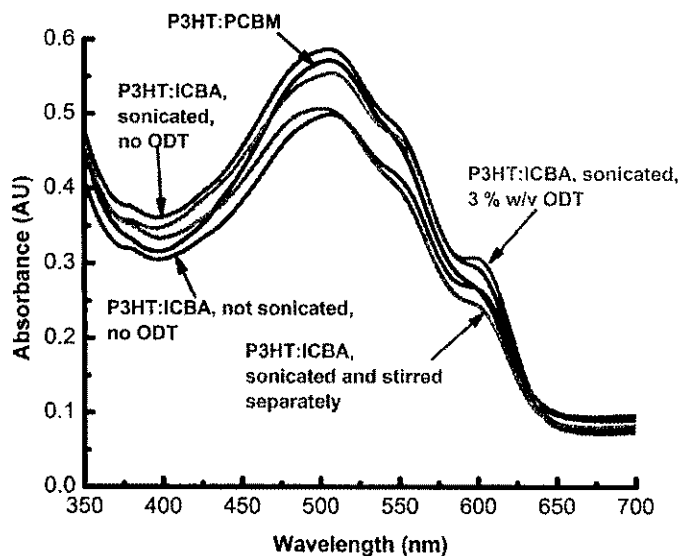


Figure 4.9: UV-Vis absorption spectra for different sonication treatments.

Table 4.8: UV-Vis peak position, intensity, and total area under curve for different sonication treatments.

Solution	Position (nm)	Intensity (AU)	Area (AU nm)
P3HT:PCBM	505.09	0.5839	117.9
P3HT:ICBA, sonicated, no ODT	504.98	0.5871	123.92
P3HT:ICBA, not sonicated, no ODT	506.99	0.4875	108.32
P3HT:ICBA, sonicated, 3% w/v ODT	506.85	0.5549	120.6
P3HT:ICBA, sonicated and stirred separately, no ODT	500.74	0.51	110.07

thin film by comparing sharpness [27]. Compared to the P3HT:PCBM solution, P3HT:ICBA solutions show much sharper shoulders. The solution using 3% w/v ODT showed the most pronounced shoulders at the indicated wavelengths indicating that ODT improves molecular ordering in the P3HT:ICBA thin film as seen previously in AFM and XRD. However, it seems that total absorption and peak intensity plays a more important

factor in determining overall PCE as the P3HT:ICBA solution which was sonicated and contained no ODT has the highest PCE and absorption.

A quick literature review shows that current results are in disagreement with several other research groups [25, 26]. Although current results for IC₆₀BA films show similar shapes to UV-Vis measurements done by these other groups, current absorption is much lower. Additionally, IC₆₀BA films should show a much more pronounced IC₆₀BA contribution at around 375 nm. I believe this discontinuity between current results and the literature comes from the fact that thin films were very nonuniform due to solubility issues as discussed previously.

Obtained spectra for the mixed solvent experiment are shown in Figure 4.8 and peak information and total absorption are given in Table 4.7. Similar discussion regarding P3HT and ICBA contributions applies. Interestingly, the pure CB solution shows a blueshifted high intensity peak and high total absorption but the lowest PCE of all ICBA solar cells fabricated. The pure CB solution also shows a less pronounced shoulder in the 540 nm region. Perhaps this decreased shoulder sharpness and increased reverse saturation current indicate a more disordered molecular structure, as seen in the XRD spectra, leading to increased recombination and a decline in photovoltaic properties. The mixed solvents show intermediate peak intensities and total absorption. Despite the decreased conjugation lengths indicated by the blueshifts observed for the mixed solvents, they show an overall improvement in absorption peak intensity and total absorption resulting in more generated excitons and thus higher J_{SC} values [28]. In agreement with the XRD results, the mixed solvents show less pronounced absorption shoulders indicating a slightly more disordered nanomorphology; however, the high J_{SC}

values brought about by reduced recombination as indicated by low J_0 values combined with improved film uniformity and high absorption balance out this slightly disordered nanomorphology resulting in better performing OSCs.

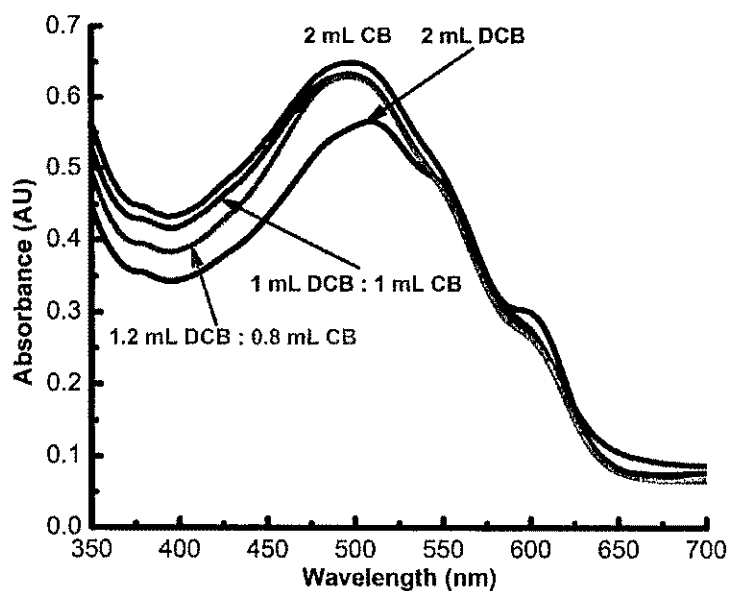


Figure 4.10: UV-Vis absorption spectra for mixed solvents.

Table 4.9: UV-Vis peak position, intensity, and total area under curve for mixed solvents.

Solution	Position (nm)	Intensity (AU)	Area (AU nm)
2 mL DCB	504.98	0.5871	123.92
1.2 mL : 0.8 mL DCB:CB	497.15	0.6297	128.1
1 mL : 1 mL DCB:CB	496.52	0.6329	134.4
2 mL CB	497.27	0.6492	137.2

4.4 Summary of Device Performance

After preceding in-depth discussion of the electrical, physical, and optical properties of the fabricated solar cells, it is helpful to present an overview of the actual effects on overall photovoltaic performance of the two conducted experiments in a concise manner. Figure 4.11 presents a summary of the relevant electrical properties including J_{sc} , V_{oc} , FF, and PCE of the devices fabricated during the sonication treatment experiment. As seen in the figure, V_{oc} increases very slightly whereas J_{sc} and FF increase more noticeably after sonication. This pattern is the same for the PCE; PCE increases after sonication. The increases in V_{oc} and FF can be attributed to less recombination in the OSC [1]. Sonicating and stirring separately results in decreased J_{sc}

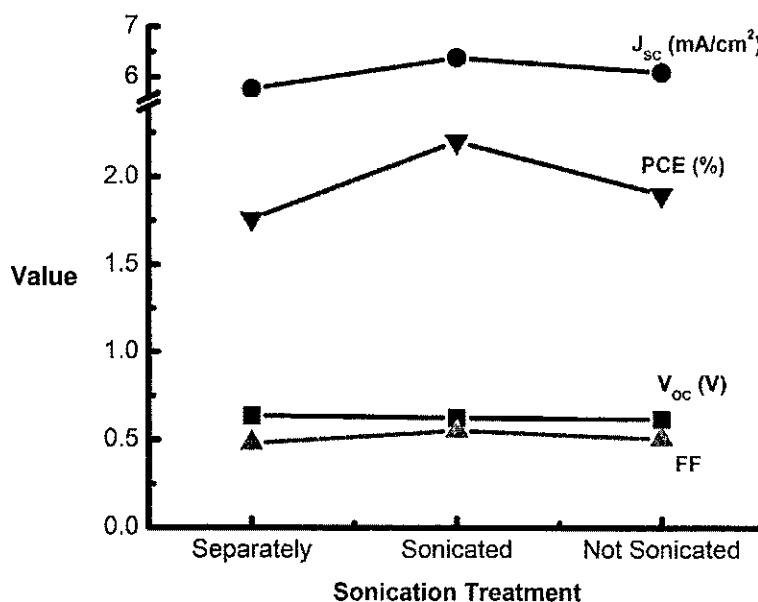


Figure 4.11: Summary of the electrical properties of the sonication treatment experiment.

and FF resulting in a decrease in PCE.

Figure 4.12 provides an overview of the physical properties for the devices fabricated during the sonication treatment experiment. As seen in Figure 4.12 (a), sonication decreases RMS surface roughness as measured by AFM. Therefore, it is possible to conclude that sonication increases the solubility of ICBA. The resulting sonicated thin film is much more uniform with fewer clusters of ICBA and less

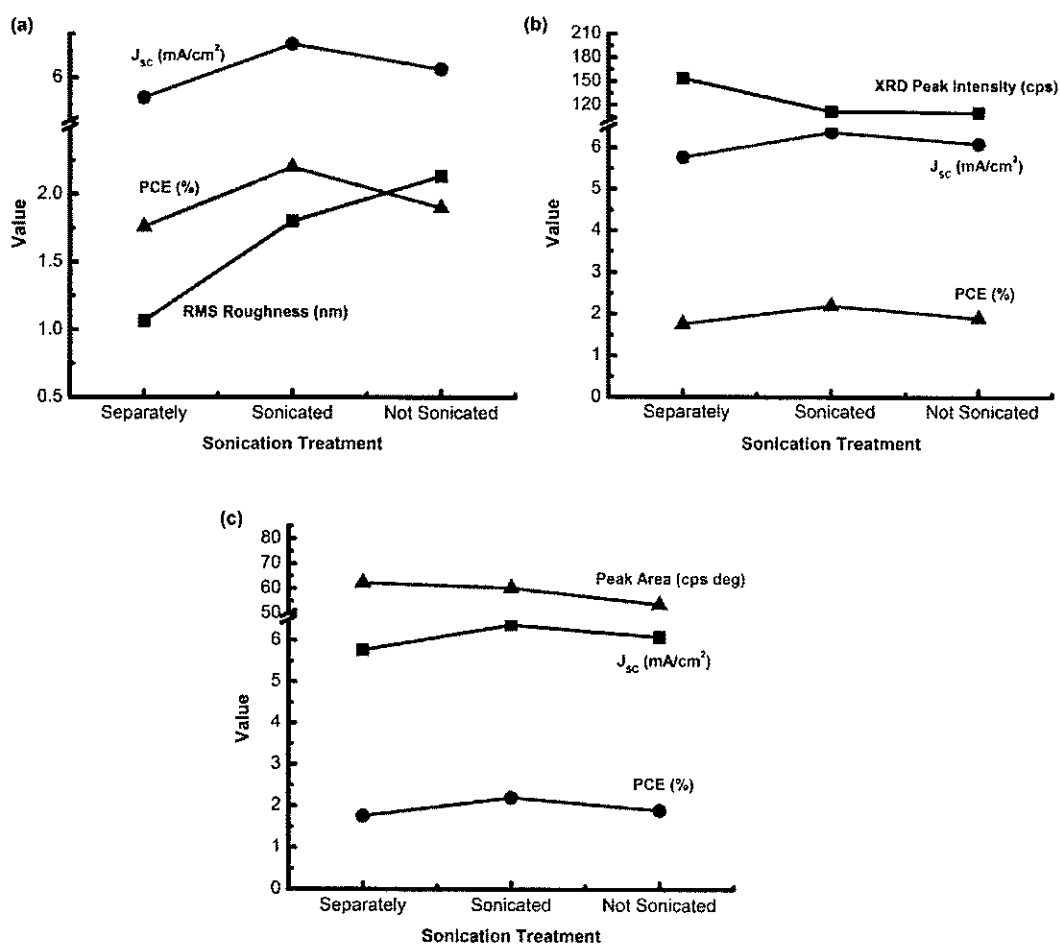


Figure 4.12: Summary of the physical properties of the sonication treatment experiment including the effect of (a) RMS roughness (b) XRD peak intensity and (c) XRD peak area.

recombination sites. As a result, using the sonicated solution results in improved J_{SC} and PCE. Despite a smoother, more uniform thin film resulting from the solution sonicated and stirred separately, a decrease in J_{SC} and PCE is observed due to optical losses described previously. Figure 4.12 (b) shows a slight improvement in the XRD peak intensity of the sonicated device as compared to the device not sonicated, but Figure 4.12 (c) shows a much more apparent improvement in XRD peak area indicating an improvement in the molecular order of the thin film. Again, the device fabricated from the solution which was sonicated and stirred separately shows superior XRD peak intensity and area but inferior photovoltaic properties due to optical losses.

Figure 4.13 summarizes the effect optical properties have on the photovoltaic performance of the solar cells fabricated for the solvent treatment experiment. We observe that sonicating the solution results in the highest peak intensity and total absorption resulting in more generated excitons and thus a higher J_{SC} and PCE. The

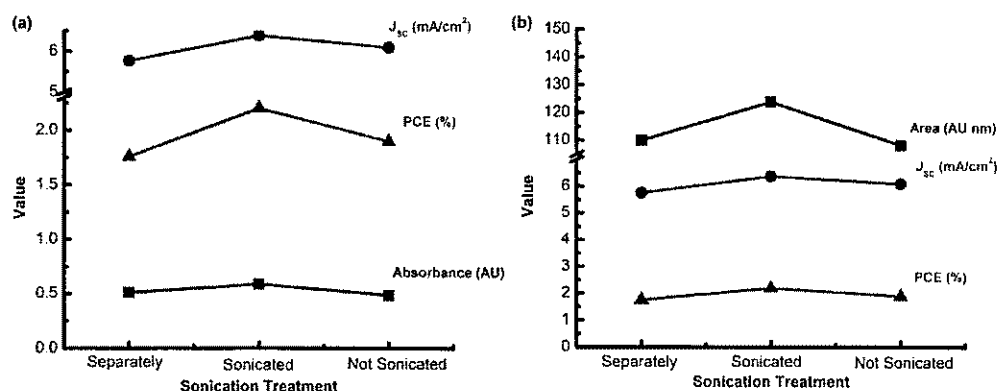


Figure 4.13: Summary of the optical properties of the sonication treatment experiment including the effect of (a) absorbance peak intensity and (b) total absorbance area.

device which used the solution which was not sonicated exhibits the lowest absorbance peak intensity and total absorption resulting in low J_{SC} and PCE. As discussed previously, the device which used the solution which was sonicated and stirred separately exhibits optical losses in absorbance peak intensity and total absorption resulting in the observed decline in photovoltaic performance. Moreover, the device which used ODT additive shows a slight decrease in absorbance peak intensity but similar total absorption as compared to the sonicated device without the additive. As such, the number of generated excitons in both devices should be similar, but due to the improved nanomorphology of the device with ODT more of those generated excitons are able to contribute to the current produced by the solar cell.

As seen above, of the three P3HT:ICBA devices fabricated during the sonication treatment experiment the device which was fabricated with the sonicated solution showed the highest PCE of 2.2%. This high PCE can be attributed to high J_{SC} and FF values resulting from improved absorption and less recombination due to good nanomorphology.

Figure 4.14 presents the electrical properties and the extracted diode parameters of the mixed solvent experiment. As seen in Figure 4.14 (a), PCE follows the same trend of J_{SC} ; increasing CB content in the mixed solvent improves J_{SC} , but then J_{SC} drops drastically with a pure CB solvent. V_{OC} and FF show little correlation to PCE. Figure 4.14 (b) shows similar patterns. Increasing the CB content in the mixed solvent results in smaller J_0 and n values, indicating lower recombination and therefore higher J_{SC} and PCE. A pure CB solvent results in a huge increase in J_0 and n indicating increased amounts of recombination resulting in a sharp decline in J_{SC} and PCE.

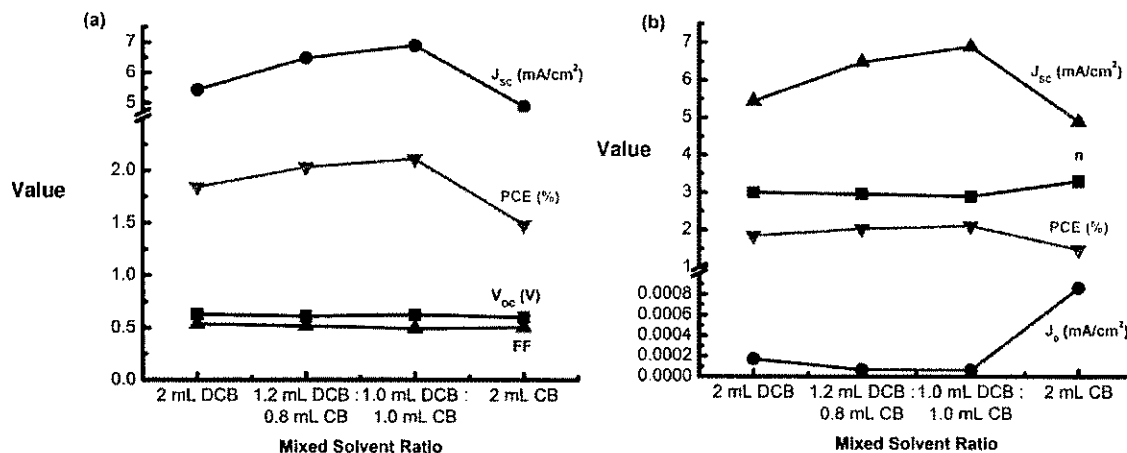


Figure 4.14: Summary of (a) the electrical properties and (b) the extracted diode parameters of the mixed solvent experiment.

Figure 4.15 shows AFM RMS roughness and XRD peak information of the mixed solvent experiment. Figure 4.15 (a) shows an almost linear decrease in RMS roughness as the content of CB is increased up to a pure CB solvent. However, J_{sc} and PCE decrease for the pure CB solvent as a result of increased recombination as seen in the diode parameters. Figures 4.15 (b) and (c) point to further recombination issues for the pure CB solvent as the XRD peak intensity and peak area are the lowest of the solvent ratios. Such a low XRD peak intensity and area indicates an undesirable nanomorphology contributing to recombination, so despite a very uniform surface with little ICBA clusters, the pure CB device performed poorly due to the above physical issues. The 1 mL DCB : 1 mL CB solvent which exhibited the highest J_{sc} and PCE shows relatively high XRD peak intensity and peak area along with a uniform surface indicating a good level of recombination.

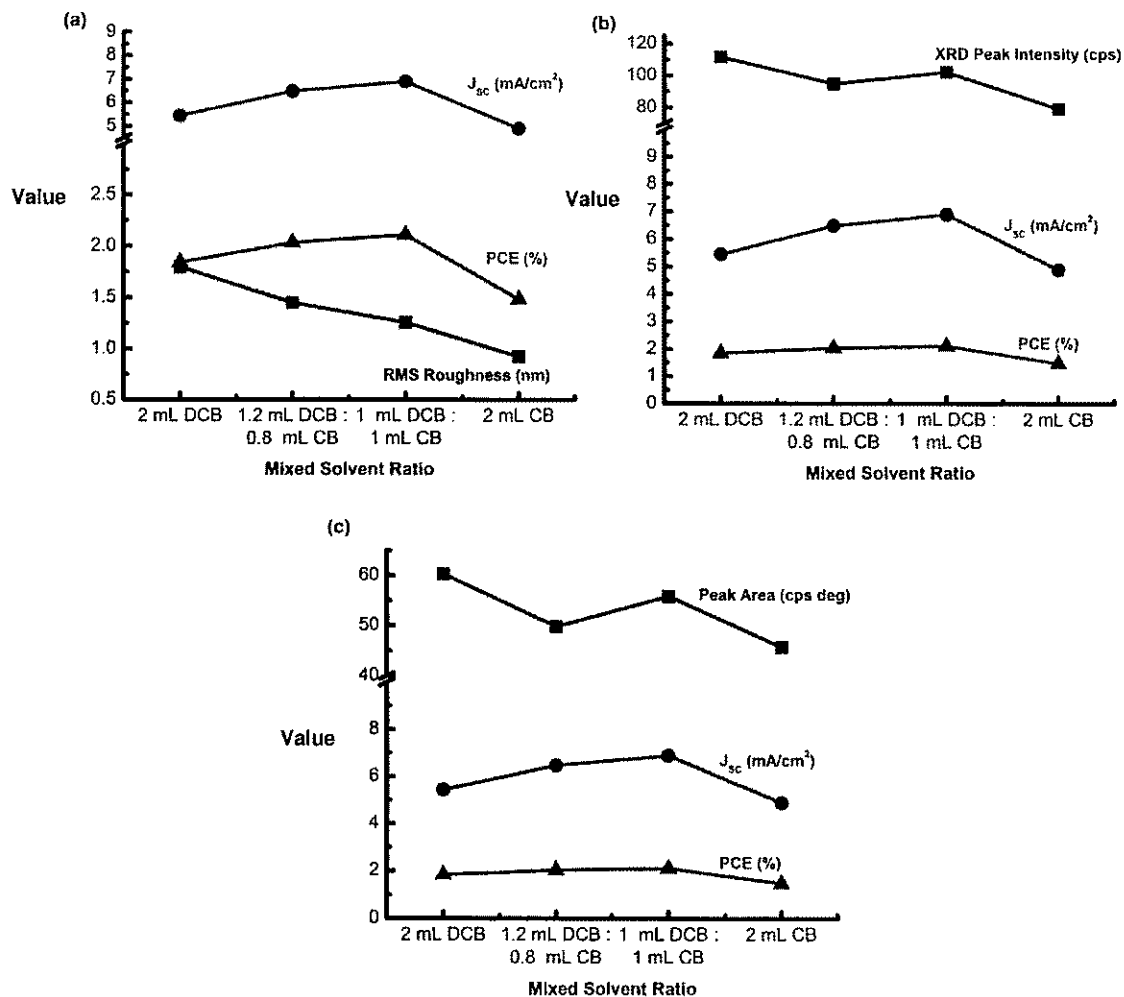


Figure 4.15: Summary of the physical properties of the mixed solvent experiment including the effect of (a) RMS roughness (b) XRD peak intensity and (c) XRD peak area.

Figure 4.16 presents a summary of the optical properties for the mixed solvent experiment. As seen in Figures 4.16 (a) and (b), increasing the CB content up to a pure CB solvent results in increasing absorbance peak intensity and total absorption. This would suggest an improvement in photovoltaic properties for even the pure CB solvent which is not observed as the device using pure CB solvent suffers from high recombination as indicated by low J_{SC} , high J_0 and n , and low XRD peak intensity and

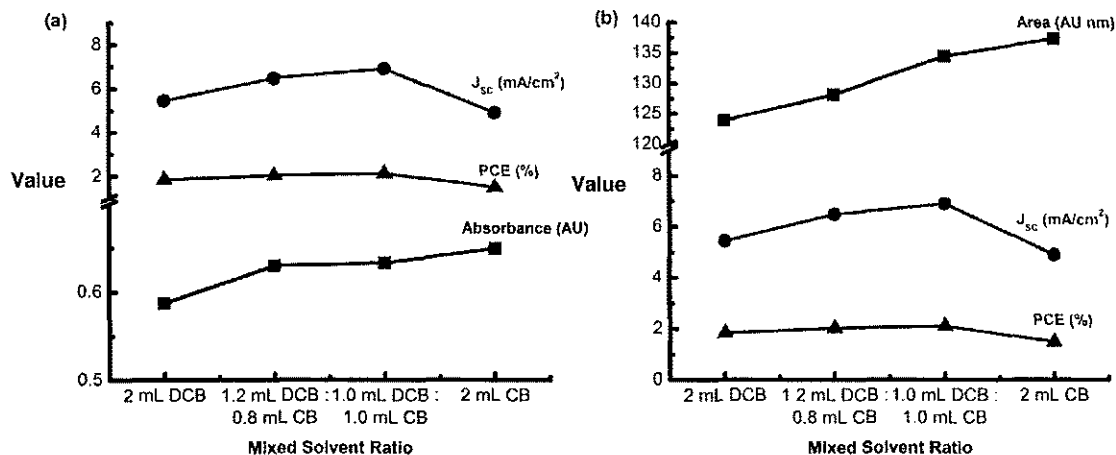


Figure 4.16: Summary of the optical properties of the mixed solvent experiment including the effect of (a) absorbance peak intensity and (b) total absorbance area.

area. However, an improvement in photovoltaic performance is observed in the mixed solvents as the higher total absorption results in more generated excitons contributing to higher currents.

Of the four devices fabricated during the mixed solvent experiment, the device using a mixed solvent with a ratio of 1.0 mL DCB : 1.0 mL CB showed the highest PCE of 2.109 %. This can be attributed to low recombination as indicated by a low J_0 and n . This low recombination is observed to be due to improved nanomorphology brought about by increased solubility resulting in relatively high XRD peak intensity and peak area. Moreover, the total number of photogenerated excitons is higher in this device as absorbance peak intensity and total absorption are higher for this device resulting in a higher number of charge carriers which can contribute to the current.

CHAPTER 5

CONCLUSION AND FUTURE WORK

5.1 Conclusion

In this thesis work, electrical, physical, and optical properties of fabricated P3HT:ICBA OSC devices were studied and compared. Various solutions were prepared to test solvent treatments in terms of the photovoltaic performance of the devices. In this thesis, two experiments were described: the sonication treatment experiment and the mixed solvent experiment. In the sonication treatment experiment, it is found that sonicating the photoactive solution improves solubility and molecular order resulting in a decrease in recombination as indicated by improved V_{OC} , FF, and XRD peaks. Additionally, sonication results in higher total absorption allowing for higher exciton generation leading to an increased J_{SC} . Further improvements can be seen using ODT solvent additive which further enhances nanomorphology. In the mixed solvent experiment, it is found that using a mixed solvent composed of 1.0 mL DCB : 1.0 mL CB results in a device with low recombination as indicated by low J_0 and n values brought about improved nanomorphology as a result of increased solubility. Similarly, this device exhibited large exciton generation due to high total absorption resulting in higher currents.

The highest observed efficiency in this thesis was 2.250% and was observed for the device utilizing a photoactive layer spin cast from a solution of 25 mg P3HT and 25 mg ICBA dissolved in 2 mL of DCB with 3% w/v ODT additive sonicated for 1 hour prior to spinning at 200 rpm and 25 °C followed by spinning at 200 rpm and room

temperature overnight. Further improvements in the devices in the lab can be achieved through process optimization as will be discussed in the following section.

5.2 Future Work

A further possible modification which can be made during the photoactive layer solution preparation step is to apply a constant electric field to the solution during the stirring step. Furthermore, the effects of applying an electric field during other steps of the fabrication process such as during annealing or during the P3HT:ICBA drying time should be explored. The literature indicates that applying such a constant field during the annealing step of fabricating OSCs results in improved molecular order as a result of dipole alignment of the polar polymer which leads to a more oriented polymer chain. It was observed that JSC increased greatly as a result of this improved molecular order [29].

Once solubility issues have been solved and a high V_{OC} has been obtained, step by step process optimization should be done to produce the most efficient P3HT:ICBA solar cell. This process optimization would seek to determine ideal processing parameters by systematically varying each step in the fabrication and comparing OSC devices made with each variable. In such a way, optimal annealing times and temperatures and layer thicknesses can be determined.

As previously mentioned, OSCs are quite instable in air. Thus, a comparative study of the time degradation characteristics of P3HT:ICBA and P3HT:PCBM is of interest. Additionally, various methods of improving device lifetime have been studied. One such method is to seal and encapsulate the device with resins such as Surlyn to prevent oxygen and water moisture from entering the device [9]. Another method uses

proper interfacial layers such as titanium suboxide (TiO_x). TiO_x has been proven to improve device stability by acting as an oxygen and water shield and to improve device efficiency by acting as an optical spacer [30, 31]. Additional interfacial layers typically used in P3HT:ICBA solar cells include Ca and LiF [11, 26]. These interfacial layers are used as electron selective transport layers to form better ohmic contacts. Use of the above interfacial layers should also be studied in the lab.

Further improvements in P3HT:ICBA solar cells can be attained through nanostructured OSC architecture as discussed in Chapter 2. Work should be done to develop the necessary nanofabrication methods to pattern P3HT and ICBA as nanorods to eliminate trapping islands and reduce recombination [15].

REFERENCES

- [1] C. Honsberg, S. Bowden, *PVCDROM*, WWW Document, (<http://www.pveducation.org/pvcdrom>) [Feb. 20, 2013].
- [2] C. J. Brabec, N. S. Sariciftci, J. C. Hummelen, *Adv. Funct. Mater.* **11**, 15-26 (2001).
- [3] C. J. Brabec, *Sol. Energ. Mat. Sol. Cells* **83**, 273-292 (2004).
- [4] H. Hoppe, N. S. Sariciftci, *J. Mater. Res.* **19**, 1924-1945 (2004).
- [5] T. L. Benanti, D. Venkataraman, *Photosynth. Res.* **87**, 73-81 (2006).
- [6] H. Spanggaard, F. C. Krebs, *Sol. Energ. Mat. Sol. Cells* **83**, 125-146 (2004).
- [7] G. Hering, "Year of the tiger," *Photon International*, March 2011, p. 208.
- [8] G. Wilson, D. Mooney, *Best Research Cell Efficiencies*, WWW Document, (http://www.nrel.gov/ncpv/images/efficiency_chart.jpg) [Feb. 20, 2013].
- [9] J. Kalowekamo, E. Baker, *Sol. Energ.* **83**, 1224 (2011).
- [10] chemBlink Inc., *Poly(3-hexylthiophene-2,5-diyl)*, WWW Document, (<http://www.chemblink.com/products/104934-50-1.htm>) [July 29, 2013].
- [11] C. Li, H. Yip, A. K. Jen, *J. Mater. Chem.* **22**, 4161-4177 (2012).
- [12] chemBlink Inc., *Methyl [6,6]-phenyl-C61-butyrate*, WWW Document, (<http://www.chemblink.com/products/160848-22-6.htm>) [July 29, 2013].
- [13] P. Boland, K. Lee, G. Namkoong, *Sol. Energ. Mat. Sol. Cells* **94**, 915-920 (2010).
- [14] chemBlink Inc., *1',1'',4',4''-Tetrahydrodi[1,4]methanonaphthaleno[1,2:2',3';56,60:2'',3'']-[5,6]fullerene-C60-Ih*, (<http://www.chemblink.com/products/1207461-57-1.htm>) [July 29, 2013].
- [15] D. Gu, H. Baumgart, G. Namkoong, *Phys. Status Solidi RRL*. **5**, 104-106 (2011).
- [16] C. Deibel, V. Dyakonov, *Rep. Prof. Phys.* **73**, 096401 (2010).
- [17] S. Lattante, A. Perulli, M. Anni, *Synth. Met.* **161**, 949-952 (2011).
- [18] S. Lin, S. Lang, J. Sun, C. Lin, in *Proceedings of the 38th IEEE Photovoltaic Specialists Conference*, 002761-002763 (2012).

- [19] G. Namkoong, J. Kong, M. Samson, I. Hwang, K. Lee, *Org. Electron.* **14**, 74-79 (2013).
- [20] R. A. Street, M. Schoendorf, A. Roy, J. H. Lee, *Phys. Rev. B* **81**, 205307 (2010).
- [21] G. Wetzelaer, M. Kuik, M. Lenes, P. Blom, *Appl. Phys. Lett.* **99**, 153506 (2011).
- [22] T. Kirchartz, B. Pieters, J. Kirkpatrick, U. Rau, J. Nelson, *Phys. Rev. B* **83**, 115209 (2011).
- [23] H. Kim, S. Ok, H. Chae, Y. Choe, *Nanoscale Res. Lett.* **7**, 56 (2012).
- [24] C. A. Lucas, in *Surface Analysis - The Principle Techniques*, edited by J. C. Vickerman, I. S. Gilmore (Wiley, West Sussex 2009) pp. 447-456.
- [25] Y. Lin, Y. Tsai, C. Wu, C. Tsai, C. Chiang, H. Hsu, J. Lee, C. Cheng, *Org. Electron.* **13**, 2333-2341 (2012).
- [26] X. Guo, C. Cui, M. Zhang, L. Huo, Y. Huang, J. Hou, Y. Li, *Energ. Environ. Sci.* **5**, 7943-7949 (2012).
- [27] J. Yun, J. Peet, N. Cho, G. Bazan, S. Lee, M. Moskovits, *Appl. Phys. Lett.* **92**, 251912 (2008).
- [28] Y. Chang, W. Su, L. Wang, *Sol. Energ. Mat. Sol. Cells* **92**, 761-765 (2008).
- [29] A. Bagui, S. S. Iyer, *IEEE Trans. Electron Dev.* **58**, 4061-4066 (2011).
- [30] K. Lee, J. Y. Kim, S. H. Park, S. H. Kim, S. Cho, A. J. Heeger, *Adv. Mater.* **19**, 2445-2449 (2007).
- [31] J. Y. Kim, S. H. Kim, H. Lee, K. Lee, W. Ma, X. Gong, A. J. Heeger, *Adv. Mater.* **18**, 572-576 (2006).

APPENDIX: COPYRIGHT PERMISSIONS / AUTHORIZATIONS

Chapter 2, Page 15, "Figure 2.6. Operation of an OSC." is reproduced from the following journal article:

C. Deibel, V. Dyakonov, Rep. Prof. Phys. **73**, 096401 (2010).

Permission to reproduce the above figure is given with the below:

Dear Matthew Samson,

Thank you for your request to reproduce IOP Publishing material.

We are happy to grant permission for the use you request on the terms set out below.

If you have any questions, please feel free to contact our Permissions team at permissions@iop.org.

I should be grateful if you would acknowledge receipt of this email.

Kind regards,

Sarah Ryder

Publishing Administrator
Email: permissions@iop.org

Conditions

Non-exclusive, non-transferrable, revocable, worldwide, permission to use the material in print and electronic form will be granted **subject to the following conditions:**

- Permission will be cancelled without notice if you fail to fulfil any of the conditions of this letter.
- You will make reasonable efforts to contact the author(s) to seek consent for your intended use. Contacting one author acting expressly as authorised agent for their co-authors is acceptable.
- You will reproduce the following prominently alongside the material:

O the source of the material, including author, article title, title of journal, volume number, issue number (if relevant), page range (or first page if this is the only information available) and date of first publication

O for material being published electronically, a link back to the article (via DOI)

O if practical and IN ALL CASES for works published under any of the Creative Commons licences the words “© IOP Publishing. Reproduced by permission of IOP Publishing. All rights reserved”

- The material will not, without the express permission of the author(s), be used in any way which, in the opinion of IOP Publishing, could distort or alter the author(s)’ original intention(s) and meaning, be prejudicial to the honour or reputation of the author(s) and/or imply endorsement by the author(s) and/or IOP Publishing.
- Payment of £0 is received in full by IOP Publishing prior to use.

Please note: IOP does not usually provide signed permission forms as a separate attachment. Please print this email and provide it to your publisher as proof of permission.

**COPIES OF ALL COPYRIGHT AUTHORIZATIONS ARE ON FILE WITH THE
OLD DOMINION UNIVERSITY REGISTRAR’S OFFICE**

VITA

Matthew Blaine Samson
Department of Electrical and Computer Engineering, KH 231
Old Dominion University
Norfolk, VA 23529
Msams002@gmail.com

Education

Master of Science in Electrical and Computer Engineering, August 2013
Old Dominion University, Norfolk, VA

Bachelor of Science in Electrical Engineering, May 2012
Old Dominion University, Norfolk, VA

Employment

Old Dominion University Applied Research Center, Jefferson Lab, Newport News, VA
Research Assistant under Dr. Gon Namkoong (May 2011-August 2013)

Fabricate and test organic solar cells. Design and carry out experiments to optimize organic solar cell efficiency. Maintain and operate various semiconductor fabrication and characterization machines including spincoaters, various vacuum pumps, a glove box, a thermal evaporator, an electron beam evaporator, a source measurement unit, a UV-Vis spectrophotometer, and a mask aligner.